Predicted CO_2 water rock reactions in naturally altered CO_2 storage reservoir sandstones, with interbedded cemented and coaly mudstone seals

Pearce J.K.[1,2*], Dawson G.W. [2], Golding S.D.[2], Southam G. [2], Paterson D.J.[3], Brink, F.[4], Underschultz, J.R.[1]

1 Centre for Natural Gas, The University of Queensland, QLD, Australia

2 School of Earth and Environmental Sciences, University of Queensland, QLD, Australia

3 Australian Synchrotron, ANSTO, Clayton, VIC, Australia

4 Centre for Advance Microscopy, Australian National University, ACT, Australia

*Corresponding author: J.pearce2@uq.edu.au

Abstract

Geological storage of CO_2 captured from industrial processes such as coal combustion or from direct air capture is part of the transition to low emissions. The Precipice Sandstone of the southern Surat Basin Queensland, Australia, is undergoing feasibility studies for industrial scale CO_2 geological storage, however regional data has so far been lacking. Reservoir drill core samples from two wells in the southern Surat are favourably quartz rich with quartz grain fracturing, silica, apatite, rutile and carbonate cements. K-feldspars are weathered with localised secondary porosity and pore filling kaolinite and illite. Layers of coal and grain compaction give vertical heterogeneity with pyrite, barite and mixed composition sulphides associated with disseminated coals in mudstones. Precipice Sandstone mercury intrusion porosities ranged from 9 – 22% with low reservoir injection threshold pressures, and QEMSCAN measured open porosity was 2 – 22%. Evergreen Formation seal porosities were 7.5 – 16% or 1 – 19% by these two methods with the smallest pore throat distribution associated with the coal rich sample. The overlying Evergreen Formation consists of clay rich sandstones, interbedded mudstones, coal layers, Fe-Mg-Mn siderite, and Mg-calcite cemented sandstones. Synchrotron XFM shows Rb mainly hosted in K-feldspars and muscovite, with metals including Mn mainly hosted in siderite. Zn and As are present in sulphides, and calcite and apatite cements mainly hosted Sr. Twenty kinetic geochemical CO_2-water-rock models were run for 30 and 1000 years. In the Precipice Sandstone reservoir variable alteration of feldspars and chlorite to kaolinite, silica, siderite and smectite were predicted with the pH remaining below 5.5. CO_2 was mineral trapped through alteration of chlorite to siderite in three of the four cases, with -0.02 to 1.43 kg/m^3

CO_2 trapped after 1000 years. Plagioclase conversion to ankerite trapped the most CO_2 at 2.6 kg/m^3 after 1000 years in calcite and siderite cemented Evergreen Formation seal. The Precipice Sandstone in both wells appears to be generaly suitable as a storage reservoir, with mineral trapping predicted to mainly occur in the overlying Evergreen Formation and in interbedded mudstones. Considering these rocks as potential natural analogues, the sequestration of metals such as Mn into siderite is likely. Mudstone and coal layers are likely to introduce baffling of CO_2 and encourage trapping, however the influence of quartz grain fracturing on migration may need future investigation. Future experimental CO_2 reaction studies are recommended, along with investigating potential CO_2 adsorption trapping in coal layers.

Keywords

CO_2 storage

Geochemical reactions

Precipice Sandstone

Evergreen Formation

Surat Basin

Coaly mudstone

1. Introduction

CO_2 capture and geological storage has been proposed as part of the solution to reduce emissions to the atmosphere and mitigate global warming. Captured CO_2 sources may include coal post combustion capture or oxyfuel firing, natural gas processing, cement or steel production, direct air capture, or blue hydrogen production (IEA, 2020; IPCC, 2005; Porter et al., 2015). Understanding the reservoir and seal rocks and their response to injected CO_2 is part of the feasibility process at potential injection sites (Carroll et al., 2013; Förster et al., 2010; Kharaka et al., 2018; Pearce et al., 2019a; Wdowin et al., 2014). Reservoir rocks generally require low reactivity or potential for clogging, high porosity and permeability and low injection threshold pressures (Bachu and Haug, 2005). A cap-rock or seal package often consisting of interbedded low porosity and low permeability shale, mudstone, or carbonate rock structurally traps buoyant supercritical CO_2 (Busch et al., 2010; Gibson-Poole et al., 2008; Pearce and Dawson, 2018). When injected subsurface

supercritical CO_2 dissolves into formation water (dissolution trapping) causing acidification it can potentially dissolve rock minerals, modifying porosity, and releasing elements to solution (Bachu et al., 1994; Johnson et al., 2011; Kharaka et al., 2006). The release of cations such as Fe, Ca, Mg, from feldspars and clays provide ions for subsequent precipitation of dissolved CO_2 as carbonate minerals such as siderite, ankerite, calcite, and dolomite, mineral trapping the CO_2 (Matter et al., 2016; Palandri et al., 2005; Pearce et al., 2021; Pearce et al., 2020). Increased concentrations of Ca, Mn, and Fe, and a sharp decrease in pH were reported in field tests injecting CO_2 into the Frio Formation sandstone in the USA (Kharaka et al., 2006). Separately, elements including Fe, Pb and As were released in a combined experimental and geochemical modelling study simulating CO_2 injection into the limestone reservoir and shale rocks of the Southwest Regional Partnership on Sequestration Pilot site (Marcon and Kaszuba, 2015). Increases in Sr concentrations and isotope ratios during CO_2 enhanced oil recovery at Salt Creek Field, Wyoming, revealed calcite and silicate dissolution, with mainly plagioclase dissolution, and smectite and calcite precipitation over 6 months (Bickle et al., 2017). During geological CO_2 storage, mineral dissolution and precipitation reactions may also modify the poro-perm characteristics, potentially affecting CO_2 injectivity and containment (Luquot et al., 2016). For example, dissolution of calcite cement from sandstones resulted in increased porosity in batch experiments with pure CO_2 or CO_2, SO_2 and O_2 gas mixtures ; or in flow through reactions with limestone (Ellis et al., 2013; Farquhar et al., 2015; Pearce et al., 2019b; Pearce et al., 2016). Information on mineral precipitation in field trials from CO_2-water-rock reactions is limited owing to the time periods involved, with information from natural analogue studies of natural CO_2 accumulations over longer time periods more accessible (Bickle et al., 2013). The Carbfix demonstration site in Iceland reported the reaction of of injected dissolved CO_2 with basalts to securely trap 50% of CO_2 and 76% of H_2S as calcite, ankerite and pyrite within 4-9 months (Matter et al., 2016). The natural alteration of chlorite and plagioclase in sandstone to trap natural CO_2 as siderite and ankerite has been reported in both South Australia and New Zealand (Higgs et al., 2013; Higgs et al., 2015). Natural mineral trapping of CO_2 as calcite, siderite, ankerite and dawsonite have also been reported in CO_2 rich coals in eastern Australia (Golab et al., 2006; Golding et al., 2013; Golding et al., 2011; Uysal et al., 2011). In the USA, calcite (and Fe-oxide) precipitation re-sequestered released metals in red bed sandstones exposed to natural CO_2 at Green River (Wigley et al., 2012). Calcite and dolomite have sequestered CO_2, with anhydrite and pyrite sequestering S in the Madison Limestone (Kaszuba et al., 2011).

Synchrotron X-ray flourescence mapping (XFM) has a strong potential application in CO_2 sequestration studies however it has so far been under utilised in underground geological storage applications (Viswanathan et al., 2012). CO_2 sequestration through mineralisation in surface mine tailings have been shown to trap potentially hazardous metals such as Ni in precipitated magnesite where XFM detected trace metals in reactants and sequestered in precipitates (Hamilton et al., 2018). XFM has also been used to detect Sr incorporated in new calcite precipitated in experiments simulating mineral trapping in beach rock formation (McCutcheon et al., 2017).

1.1 Study site

The Surat Basin and Clarence Morton Basin in Queensland form part of the Great Artesian Basin (GAB) an important water resource in Australia (Figure 1). Northern regions of the Surat Basin e.g. the Glenhaven site near Wandoan have been previously investigated for demonstration scale CO_2 storage (Pearce et al., 2019b). Regions in the south of the basin are expected to be more suitable, including for example the lower quality reservoir water, depth, and proximity to power stations and infrastructure. Initial sources of CO_2 have been proposed from coal fired power stations with post combustion capture (PCC). The Millmerran and Kogan power stations are in the region. The Calide Oxyfuel capture pilot plant in Queensland, Australia, also investigated capture from oxyfuel coal combustion (Liu et al., 2016). The Surat Basin also has a long history of oil and gas production, and other industies, that may provide further options, for example, with the future potential of blue hydrogen production i.e. production from natural gas with CO_2 storage (Baublys et al., 2021; Pearce et al., 2019a; Underschultz et al., 2016). Ammonia production, and direct air capture (DAC) for example are other future options. Most notably the Moonie Oil Field to the south of the Moonie Goondiwindi fault zone has produced oil from sandstones in both the Precipice Sandstone and Evergreen Formations since the 1960s as Australia's first commercial hydrocarbon discovery. Gas was first discovered in 1900 at Roma, with commercial quantities not produced until 1969 from the Roma region. Underschultz et al. (2016) further describe hydrocarbon indicators mainly clustered around major fault zones in the Precipice Sandstone, Evergreen Formation, and overlying strata such as the Hutton Sandstone, and Walloon Coal Measures that host coal seam gas (Underschultz et al., 2016). Golding et al. (2016) reported natural carbonate cementation related to hydrocarbon, CO_2 and hydrothermal fluid migration associated with fault zones (Golding et al., 2016). The

Bowen Basin that underlies the Precipice Sandstone also hosts conventional and unconventional oil and gas (Hamilton et al., 2020).

The Jurassic Precipice Sandstone is the proposed injection reservoir, and the Evergreen Formation the seal (Figure 1) (La Croix et al., 2019a). Allocation of the drill cores in this study to the Precipice Sandstone reservoir follows recent stratigraphic nomenclature (Bianchi et al., 2018; He et al., 2019; La Croix et al., 2019b; Martin et al., 2018; Wang et al., 2019). The overlying interbedded sandstones and mudstones of the Evergreen Formation are overall considered a sealing package and the sedimentary facies have been described previously (La Croix et al., 2019a). The Southern Surat Basin has been predicted to be more prospective than the north for larger industrial scale CO_2 storage. This is partly owing to greater storage depths in the south, proximity to CO_2 sources, and also being geographically further from regions where water is extracted for agriculture and stock from the Precipice Sandstone reservoir or overlying aquifers such as the Hutton Sandstone (Hodgkinson and Grigorescu, 2012; Wolhuter et al., 2019). Research directed at CCS in the southern Surat Basin however has been previously limited to pre-feasibility studies. Separately, an appraisal well for CCS has also very recently been drilled west of the Moonie oil field in the southern Surat Basin. During this research project available data on drill core, including detailed mineral and element content was found to be very limited in the southern Surat Basin (Grigorescu, 2011). This study therefore characterised drill core from two available open access wells located in the southern Surat Basin located near the Moonie Goondiwindi fault zone, and to the east towards the Clarence Morton Basin entrace (Figure 1).

The aim of this study was to characterise available reservoir and seal core in the southern Surat Basin for minerals, associated element content including metals, porosity, and pore throats, and to use the data together with existing water chemistry data to predict potential subsurface reactions if CO_2 was injected. The potential for mineral trapping, the most secure form of CO_2 storage in different rock packages was assessed.

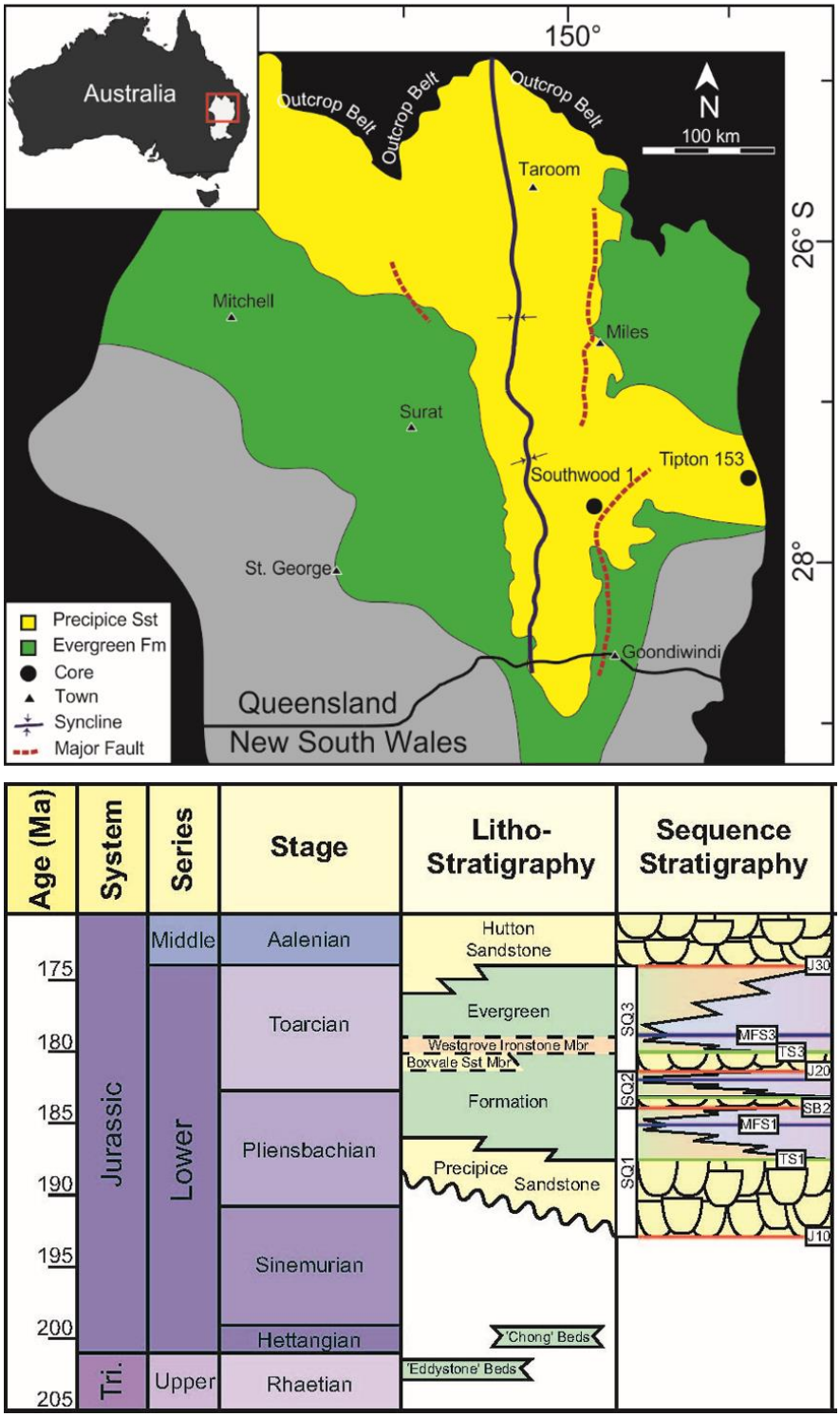

157

158 Figure 1: Map showing the Southwood 1 well and the Tipton 153 well where the yellow area
159 is showing the extent of the Precipice Sandstone. The litho- and sequence-stratigraphy of
160 the Precipice Sandstone reservoir and Evergreen Formation seal pair is shown below,
161 modified from La Croix et al. (2019a).

162

2. Methods

Drill core was sampled from the Southwood 1 well core drilled ~ 15 km to the west of Moonie, QLD, Australia, just north of the Moonie Goondiwindi fault zone (Lat. -27.709532, Long. 150.321666). Precipice Sandstone and Evergreen Formation was sampled at various depths where limited core was available as outlined in Table 1. The available core was mainly sandstone, with a dense mudstone layer also sampled. Drill core was also sampled from the Tipton 153 well core drilled ~ 20 km southwest of Dalby, QLD, Australia (Lat. -27.358606, Long. 151.153092). Core from various depths of the Precipice Sandstone and Evergreen Formation was sampled (Table 1, and supplementary material).

Mercury injection capillary pressure porosimetry (MIP) was performed on selected core samples from Southwood 1 well (Table 1) and provided porosity and pore throat distributions. These were performed at Adelaide School of Petroleum on a Micrometrics Autopore V and conformance corrected. Note that MIP is a destructive technique with adjacent core subsamples used taken as close as possible to those used in thin sections. Therefore, natural heterogeneity may influence comparisons between different porosity quantification methods. An automated scanning electron microscopy and energy dispersive spectroscopy (SEM-EDS) mineral quantification method, QEMSCAN, was used for mineral and open porosity quantification (Pirrie et al., 2004; Wunsch et al., 2014). QEMSCAN was performed with a 5 µm step size and 2000 X-ray counts per pixel on carbon coated polished thin section areas of drill core at the Centre for Advanced Microscopy, Australian National University. Seven samples of Precipice Sandstone and Evergreen Formation core from the Southwood 1 well, and eight samples from the Tipton 153 well were run (Table 1, and supplementary material). Thermo Fisher iMeasure and iDiscover software were used for data acquisition and frame stitching, with the final mineral identification and modal fraction subsequently performed using ThermoFisher Nanomin.

SEM-EDS was performed in backscatter electron detection (BSE) mode on polished thin sections using a TM3030 and a Brucker EDS at UQ to detect minor minerals, semi quantitative compositions, surface textures, clay habit, and weathering to supplement the model input data. Rock lithium borate fusions, loss on ignition (LOI), and total acid digestions were performed in the UQ Environmental Geochemistry Laboratory on powdered core samples to determine the total content of a wide range of elements, with standard methods. Major elements were determined by inductively coupled plasma optical emission spectroscopy (ICP-OES) with compositions reported as percentage oxides with an error of

196 less than 5% (Perkin Elmer Optima 3300 DV ICP-OES instrument with a 3σ detection limit of
197 0.001 mg l^{-1}). Loss on ignition was also determined, along with minor and trace element
198 analysis by acid digestion (HCl-HNO_3) and inductively coupled plasma mass spectrometry
199 (ICP-MS) on a Thermo Fisher Series Xi quadrupole ICP-MS (with an error less than 10%).

200 Synchrotron X-ray Fluorescence Microscopy (XFM) was performed on the Southwood 1 well
201 Precipice Sandstone 1994.13 m core, and the Tipton 153 well core Precipice Sandstone
202 1067.92 m and Evergreen Formation 1015.0 m samples. XFM was performed at the
203 Australian Synchrotron XFM beamline, Clayton, Victoria, to measure trace metals at high
204 resolution in specific minerals (Ryan et al., 2014). The core samples were prepared as 30 µm
205 polished thin sections on fused quartz slides (Queensland University of Technology). Quartz
206 slides were used since standard glass slides may contain a background of elements (including
207 As) that can interfere with the analysis. Thin sections were attached with Mylar tape to a
208 Perspex plate sample holder and mounted to the instrument translation stage. Scanning
209 fluorescence microscopy was performed on-the-fly with an X-ray beam (18.5 KeV) focused
210 with Kirkpatrick-Baez mirrors to ~ 2µm, and the Maia detector, to produce fluorescence
211 maps. A range of major, minor and trace metals (Fe, Ca, Mn, K, Zn, Ti, Ni, Cr, Pb, As, Sr, Zr,
212 Rb) were detected first in low resolution scans over the thin section, followed by scans over
213 smaller areas of interest at up to 2 µm spatial resolution and 10 msec/pixel dwell time. Foil
214 standards were run daily to calibrate elemental concentrations, with the instrument
215 described in detail previously (Howard et al., 2020; Paterson et al., 2011; Ryan et al., 2010).
216 False colour images of concentration distributions, and quantified concentrations over
217 mineral areas were generated from the raw data with GeoPIXIE (Ryan et al., 2014).
218 Subsequently SEM-EDS was also performed on the same thin section areas scanned by XFM
219 to confirm which minerals were present in the scanned area.

220 Kinetic geochemical models were run using the react module of Geochemist Workbench 11
221 (GWB), with the thermodynamic database based on EQ3/6, and minerals entered as script
222 files as described in detail previously (Bethke and Yeakel, 2012; Delany and Lundeen, 1989;
223 Pearce et al., 2015). Equilibrated initial water chemistry from reported formation water data
224 (supplementary material), and a water-rock ratio based on porosity was used (Feitz, 2014).
225 A limitation for the Southwood 1 well was that the closest available water chemistry sample
226 was from a bore some 40 km northeast in the Precipice Sandstone at 1245 m (water
227 chemistries are given in supplementary material). In addition, a second equilibrated water
228 chemistry was used that was geographically closer (~ 5 km south) but on the other side of
229 the fault zone and in an oil field (Moonie oil field, Precipice Sandstone, 58 sands). The

second water chemistry had a more Na-bicarbonate character. Although neither water chemistries were ideal in terms of position, this reflects the low availability of data in the region, and hence we tested models with both water chemistries to see the effect on predicted pH. A fugacity of CO_2 for a reservoir pressure (20 MPa) and temperature (70°C) was used for Southwood 1, and a pressure and temperature of 12 MPa and 60°C for Tipton 153 calculated from (Duan and Sun, 2003). Models were run for 30 and 1000 years. Models for Southwood 1 were additionally run for 1000 years with half of the CO_2 fugacity to simulated potential plume edges or areas where CO_2 had migrated away. Separately, select models of the finer grained sandstones and mudstones were run over 1000 years with reactive surface areas 10 times lower than the base case to investigate the effect of lower fluid accessibility to mineral surfaces.

Mineral amounts were based on the rock sample QEMSCAN characterisation supplemented by SEM (and previous XRD) and upscaled to 10 kg of rock (supplementary material). Reactive surface area values used are given in the supplementary material. The kinetic and thermodynamic parameters were from an existing database (Palandri and Kharaka, 2004). Siderite, ankerite, illite and chlorite however were from different sources (Köhler et al., 2003; Lowson et al., 2007; Steefel, 2001), as described previously (Pearce et al., 2015; Pearce et al., 2019c). Siderite and chlorite had an Fe-Mg composition based on core SEM-EDS observations. Fe-rich chlorite (Fe:Mg 3:1), ankerite ($Ca_{0.5}Fe_{0.35}Mg_{0.15}$) and siderite ($Fe_{0.9}Mg_{0.1}$) compositions were used as input. The overall predicted net amount of CO_2 mineral trapped was calculated using the model outputs with a previously described method (Watson and Gibson-Poole, 2005). The general modelling methods were similar to methods used for the north of the basin to enable comparison (Pearce et al., 2021; Pearce et al., 2020).

3. Results

3.1 Drill core mineral and porosity characteristics

Southwood 1 well

The four deepest sampled cores were from the Precipice Sandstone, the potential reservoir. The 4 shallower cores sampled were from the Evergreen Formation. The deepest sampled core from Southwood 1 1994.13 m had the highest MIP porosity (Table 1), however the pore throat distributions show that this is made up of mainly pore throats smaller than 10 µm

(Figure 2). This is consistent with the low open porosity measured in QEMSCAN on the thin section. This sandstone was fine grained and contains the highest Al, Fe, Ti, Mg, Mn, Li, V, Ni, An, Zr, Rb, Sr, U and Pb whole rock content (Table 2, Table 3). This depth section was more fine grained and had the highest siderite cement content of 3%, with 5% K-feldspar, and kaolinite filling intergranular pores (Figure 3A, and supplementary material). QEMSCAN minerals components are given in supplementary material Table S4. Feldspars were highly corroded creating secondary porosity, and altered to kaolinite and illite filling intergranular pores. Siderite cements had an Fe-Mg-Mn +/- Ca composition, and an unusual texture of slender rhombs, filling both intergranular pores and corroded feldspar. Associated delicate rutile cements, and mixed apatite, barite and phosphate containing cements were also identified using SEM EDS (Figure 4A,B).

Moving up core, the next three Precipice Sandstone cores sampled at 1993.47 m, 1992.93 m, and 1987.64 m were more quartz rich with variable grain sizes and larger pore throats (Figure 3B, C and supplementary material). Mercury injection threshhold pressures were relatively low indicating a good potential reservoir (Table 1). Previous data reported for permeability of the closest core depth sections indicate these are from higher permeability zones of 75 -219 mD (supplementary material). Core from 1993.47 m had thin mud laminations and contained a mud rip up clast (Figure 4 C and supplementary material). Several cores contained fractured quartz grains (Figure 3 C, Figure 4 D,E). The sample from 1987.64 m had poorly sorted quartz grains and the highest incidence of parallel and perpendicual fractured quartz grains occasionally cemented with kaolinite. In addition it contained silica cements including a vein (Figure 4E,F).

Generally the highest Sr, Li, Zn, Zr, Mn and Rb concentrations were in the deepest Precipice Sandstone core from 1994.13 m, with the lowest quartz content and most kaolinite, illite and siderite cement. The lowest total Rb concentrations were in the two cores with the lowest K-feldspar and illite contents 1987.64 and 1992.93 m. The six drill cores that were characterised by MIP had a wide range of porosities and pore throat size distributions (Figure 2).

The Evergreen Formation 1957.73 m core contained mudstone sections, and a higher and bimodal threshold pressure indicating sealing capacity, with 7.5% porosity and pore throat diameters mainly below 0.1 µm (Table 1, Figure 1). The small pore throats were likely associated with the coal and kaolinite and illite/smectite clay rich matrix (Figure 5A, D, supplementary material). Dense Fe-Mg-siderite, rutile, sphalerite and pyrite cements were

present, with zircon. Crystalline pyrite, siderite and FeZn-sulphide cements were associated with dispersed coal (Figure 5E, supplementary material). The Evergreen Formation sandstone core from 1956.21 m contained a higher portion of clays, and K-feldspar than the Precipice Sandstone (Figure 5, and supplementary material). Fe-Mg-Mn +/-Ca siderite slender rhombs and rutile cements often filled the secondary porosity in corroded K-feldspar (Figure 6A, B, supplementary material) indicating that they likely were precipitated after the feldspar alteration. Framboidal pyrite was associated with organic matter, and some quartz grain fracturing was also present. The Evergreen Formation from 1952.85 m contained vertical heterogeneity from coal layers (Figure 5C, supplementary material). Barite cements were associated with coal layers (Figure 6C, D). With zircon, K-feldspar and kaolinite between compacted and fractured quartz. K-feldspar was variably corroded with siderite and kaolinite filling K-feldspar and intergranular porosity (Figure 6E, F).

Table 1: Formation and depth of all Southwood 1 well cores, and below Tipton 153 well cores. P indicates the Precipice Sandstone reservor, and E the Evergreen Formation seals. Measured core porosity (%) and threshold pressure from MIP, with grain density from He. Open porosity determined by QEMSCAN on a thin section area is also given, * indicates where the value may be skewed by lost grains in the thin section.

Well	**Formation**	**Depth (m)**	**MIP porosity %**	**Grain density g/cc**	**Threshold pressure psi**	**QEMSCAN porosity %**	**Sample #**
Southwood 1	E	1952.85	16.10	2.17	6	18.59	429
Southwood 1	E	1954.99	-			12.04	430
Southwood 1	E	1957.73	7.50	2.19	48, 2345 bimodal	-	6423
Southwood 1	E	1956.21	9.71	2.20	113	6.90	6418
Southwood 1	P	1987.64	9.09	2.21	8.5	18.58*	432
Southwood 1	P	1992.93	14.57	2.19	4, 59 bimodal	21.90*	433
Southwood 1	P	1993.47	-			10.86	434
Southwood 1	P	1994.13	21.27	2.04	39	4.46	435

Well	**Formation**	**Depth (m)**	**QEMSCAN porosity %**	**Sample #**
Tipton 153	E	1015.00	0.69	406

Tipton 153	E	1020.89	1.65	407
Tipton 153	E	1024.23	1.63	408
Tipton 153	P	1032.35	21.61*	410
Tipton 153	P	1033.88	11.01	412
Tipton 153	P	1066.00	1.82	420
Tipton 153	P	1067.92	4.52	422
Tipton 153	P	1093.00	16.55	425

315

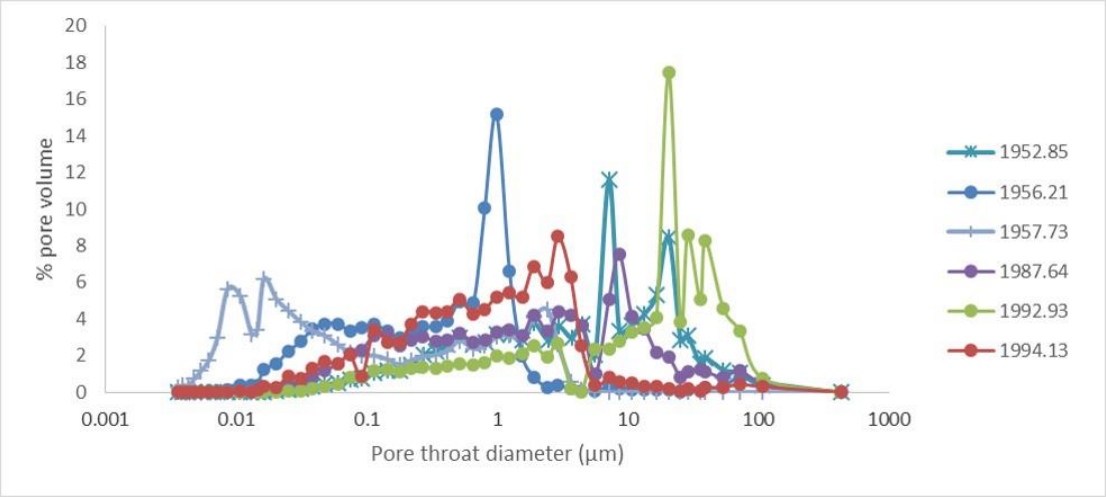

316

317 Figure 2: Pore throat diameter distributions of Southwood 1 core samples from MIP. The
318 shallowest three depths in blue are from the Evergreen Formation.

319

320 Table 2: Southwood 1 core major element composition reported as % oxide, and loss on
321 ignition (LOI).

Depth (m)	%H_2O	%LOI	Al_2O_3	CaO	Fe_2O_3	K_2O	MgO	MnO	Na_2O	P_2O_5	SiO_2	TiO_2
1952.85	0.08	1.60	4.26	0.08	0.72	0.97	0.11	0.01	0.06	0.01	91.91	0.18
1954.99	0.08	1.86	5.61	0.07	0.63	1.30	0.12	0.00	0.06	0.02	90.50	0.21
1987.64	0.02	1.10	3.33	0.02	0.14	0.45	0.03	0.00	0.03	0.02	94.63	0.22
1992.93	0.03	0.82	2.25	0.06	0.14	0.29	0.02	0.00	0.04	0.03	96.27	0.05
1993.47	0.08	1.80	6.35	0.03	0.18	0.73	0.06	0.00	0.05	0.01	90.45	0.25
1994.13	0.18	4.17	9.98	0.05	3.56	1.16	0.20	0.09	0.06	0.03	80.15	0.44

322

323 Table 3: Southwood 1 core total minor and trace element content including REE (mg/kg)
324 from total acid digestion. Data for the Tipton 153 core are given in supplementary material.

depth (m)	Li	Be	B	Sc	V	Cr	Co	Ni	Cu	Zn	Ga	Ge
1952.85	16.18	0.49	34.89	6.81	18.06	15.32	4.72	9.94	8.60	26.44	4.63	1.37
1954.99	19.63	0.54	29.85	6.92	22.01	14.19	2.95	5.42	4.27	20.53	5.66	1.21
1987.64	8.21	0.44	13.38	4.11	11.31	14.75	3.24	4.34	4.83	4.71	4.04	0.37
1992.93	11.14	0.27	3.27	1.93	6.52	9.67	1.03	3.59	13.16	14.30	2.54	0.76
1993.47	9.71	0.82	19.60	6.68	25.24	27.86	2.30	6.69	12.12	18.24	8.43	1.07
1994.13	58.83	1.40	72.85	18.02	51.88	24.34	7.49	18.04	6.70	38.32	12.05	1.78

325

depth (m)	Rb	Sr	Y	Zr	Nb	Mo	Ag	Cd	Sn	Sb	Cs	Ba	La
1952.85	103.57	23.63	11.64	39.62	3.43	0.33	0.05	0.08	1.67	0.39	1.18	169.24	7.61
1954.99	139.83	25.12	12.81	44.53	4.64	0.52	0.06	0.07	1.20	0.29	1.36	226.30	8.07
1987.64	67.16	18.50	13.38	59.33	4.27	0.11	0.06	0.08	1.61	0.32	1.10	59.35	7.89
1992.93	41.27	13.56	6.53	18.65	1.15	0.18	0.04	0.04	1.34	0.20	0.84	49.29	6.57
1993.47	120.17	31.64	17.28	92.24	6.28	0.15	0.09	0.10	3.37	0.44	2.07	104.63	18.44
1994.13	188.46	63.26	23.68	102.16	9.02	0.45	0.09	0.12	2.85	0.54	2.01	162.43	17.69

326

depth (m)	Pr	Nd	Sm	Eu	Gd	Tb	Dy	Ho	Er	Tm	Yb	Ce
1952.85	1.99	7.35	1.49	0.38	1.42	0.19	1.12	0.23	0.71	0.11	0.74	16.25
1954.99	1.94	6.91	1.41	0.43	1.46	0.22	1.26	0.25	0.78	0.12	0.78	16.38
1987.64	1.98	6.97	1.39	0.26	1.36	0.20	1.27	0.26	0.80	0.12	0.82	15.77
1992.93	1.56	5.32	1.09	0.15	0.99	0.13	0.66	0.13	0.39	0.06	0.39	13.00
1993.47	4.68	15.41	2.80	0.38	2.43	0.34	1.83	0.35	1.06	0.16	1.10	39.12
1994.13	4.37	15.50	3.00	0.68	2.88	0.40	2.35	0.47	1.46	0.22	1.50	37.55

327

Depth (m)	W	Tl	Pb	Lu	Bi	Th	U	As	Se	Hf	Ta
1952.85	1.41	0.59	9.15	0.13	0.05	7.14	0.63	6.06	0.24	1.16	0.73
1954.99	1.05	0.32	10.56	0.12	0.05	8.31	0.76	3.46	0.23	1.25	0.94
1987.64	0.79	0.15	5.50	0.13	0.04	9.09	0.89	3.04	0.21	1.75	0.89
1992.93	0.73	0.08	5.30	0.08	0.04	6.88	0.43	1.51	0.19	0.58	0.32
1993.47	1.26	0.21	12.92	0.19	0.53	24.27	1.57	4.37	0.47	2.57	1.32
1994.13	1.51	0.35	15.44	0.24	0.09	16.99	1.64	5.44	0.47	3.05	1.80

328

329

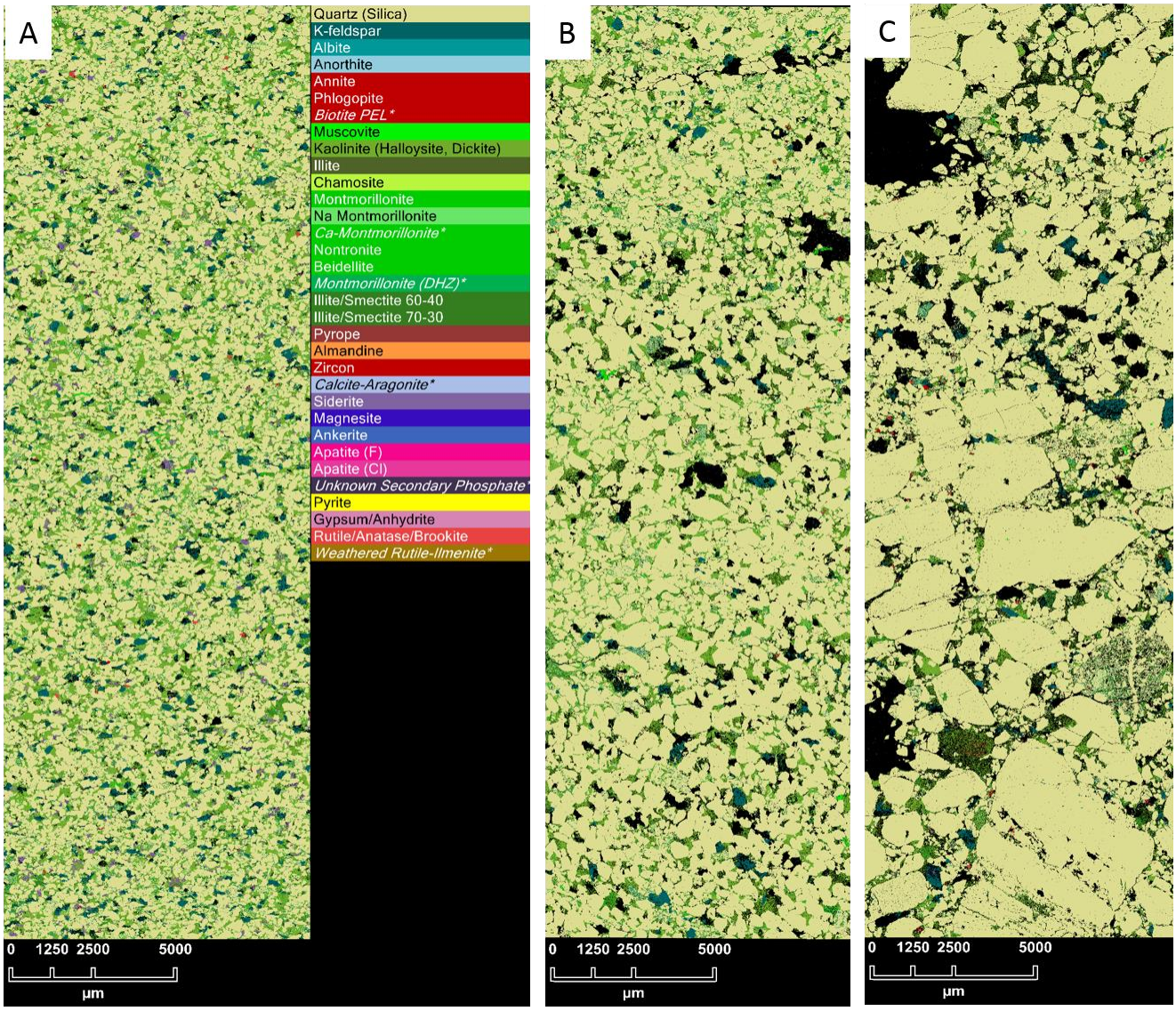

330

331 Figure 3: QEMSCAN images of drill core thin section areas from Southwood 1 reservoir
332 Precipice Sandstone. A) Fine grained 1994.13 m with some siderite cements, B) 1993.47 m,
333 C) quartz grain fracturing and silica cements in 1987.64 m. Additional core depth sections
334 are shown in supplementary material.

335

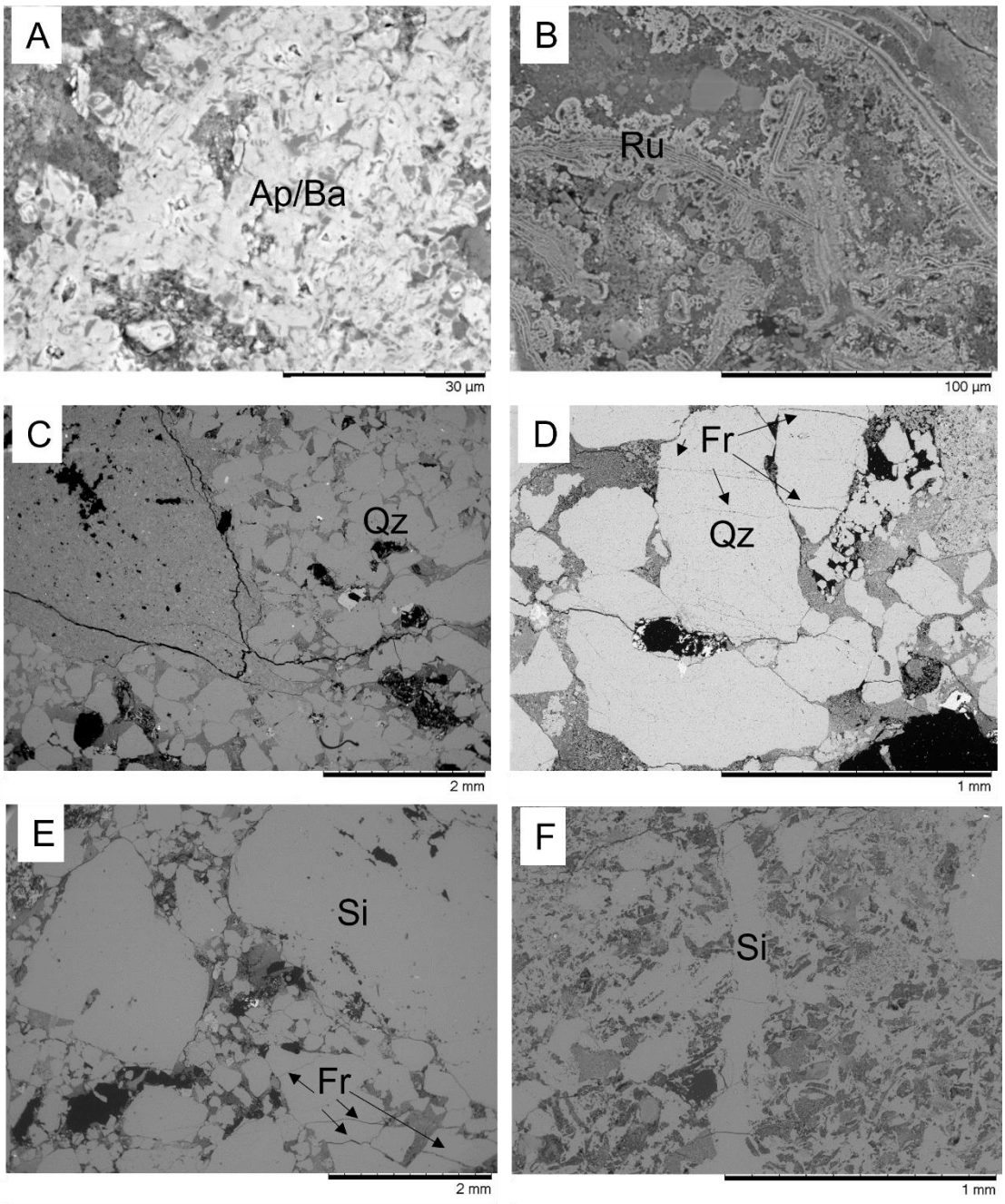

336

337 Figure 4: SEM images of Southwood 1 reservoir Precipice Sandstone. A) Mixed apatite,
338 phosphate bearing, and barite cements in 1994.13 m. C) Delicate rutile cements in 1994.13
339 m. C) Mud rip up clast and D) fractured quartz grains in 1993.47 m. E) Fractured and poorly
340 sorted quartz grains and silica cements in 1987.64 m, and F) silica vein and cement with
341 some horizontal fracturing in 1987.64 m. Qz = quartz, Si = silica cement, Ap = apatite, Ru =
342 rutile, Ba = barite, Fr = fracture.

343

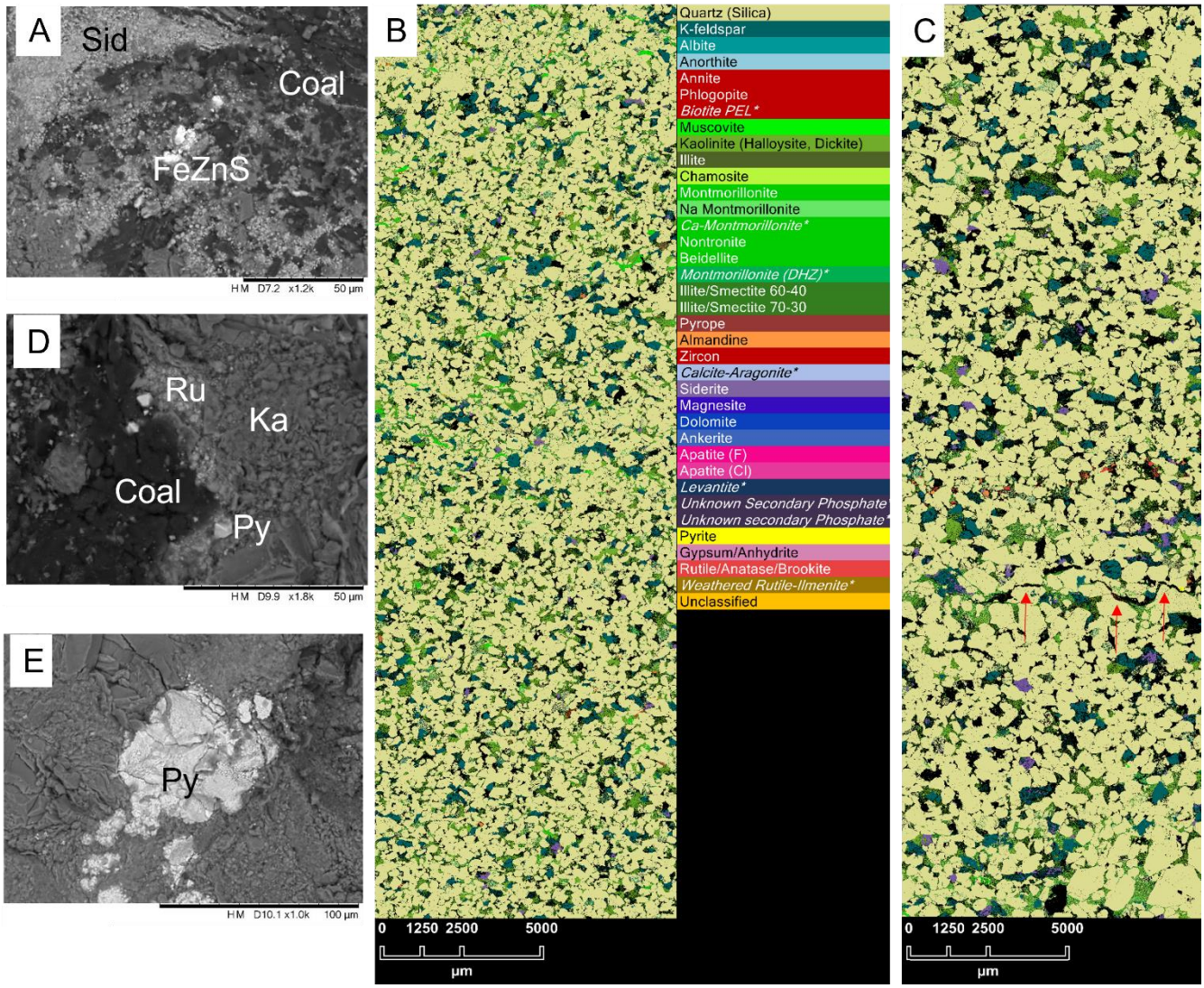

Figure 5: SEM and QEMSCAN images of drill core thin section areas of Southwood 1 seal Evergreen Formation. A) Coal, siderite and Fe-Zn-sulphide in a clay matrix in 1957.73 m. B) QEMSCAN image of 1954.99 m, C) QEMSCAN image of 1952.85 m with red arrows indicating a coal layer. D) Coal, rutile, crystaline pyrite and kaolinite in 1957.73 m, E) pyrite cement in 1957.73 m. Sid = siderite, FeZnS = FeZn-sulphide, Ka = kaolinite, Ru = rutile, Py = pyrite.

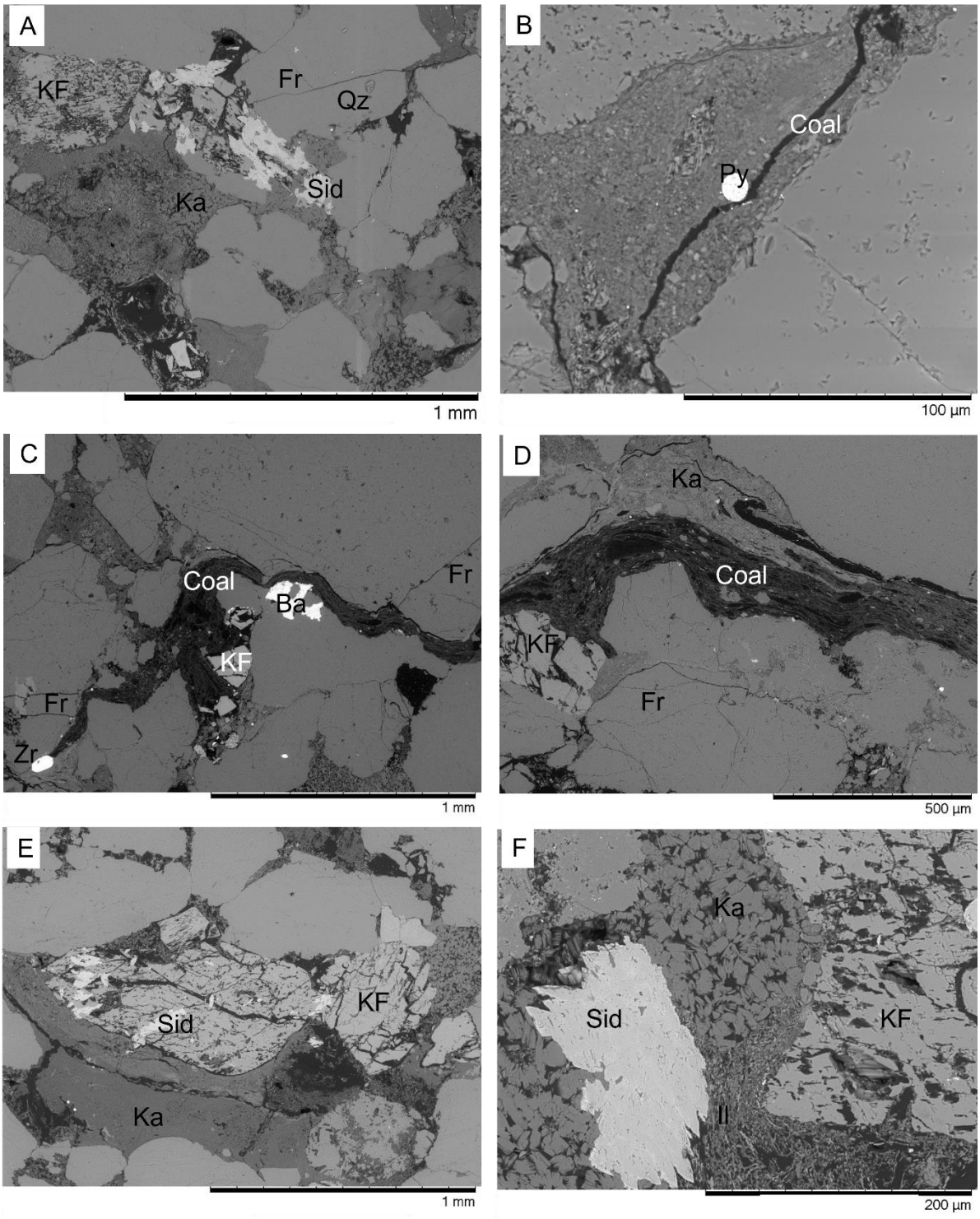

352

353 Figure 6: SEM images of Southwood 1 seal Evergreen Formation. A) fractured quartz,
354 siderite infilling corroded K-feldspar, and pore filling clays in 1956.21 m, and B) framboidal
355 pyrite and organic matter in illite in 1956.21 m. C) 1952.85 m coal layer with barite
356 cement, K-feldspar, zircon, and fractured quartz grains. D) Coal layer with pore filling
357 kaolinite and quartz grain fracturing 1952.85 m. E) Siderite filling corroded K-feldspar, with
358 associated kaolinite, and silica cement in 1952.85 m, and F) siderite cement, and corroded K-

feldspar, with pore filling blocky kaolinite and illite in 1952.85 m. Qz = quartz, Sid = siderite, Ka = kaolinite, KF = K-feldspar, Py = pyrite, Zr = zircon, Ba = barite, Fr = fracture.

Tipton 153 well

QEMSCAN was performed on eight of the Tipton 153 core thin sections (Table 1), five from the Precipice Sandstone reservoir, and three from the Evergreen Formation seals. The Precipice Sandstone 1093.0 m and 1032.25 m samples were quartz rich and poorly sorted with open porosity (16.55 – 21.61%), occasional fractured quartz grains and minor kaolinite (Table 1, Figure 7, and supplementary material). Quartz grain fractures in 1093.0 m were often filled with kaolinite (Figure 8). Two low porosity sections from 1066.00 and 1067.92 m are part of a mudstone layer that has been observed in other wells in the basin but is thought to be discontinuous. The 1067.92 m sample was clay rich and contained 4% pore filling siderite cements, muscovite and illite layers with Ti signatures, zircon, and layers of quartz grain compaction. Silica cements and corroded quartz grains infilled by siderite were present, along with rutile cement and quartz grains with perpendicular fractures (supplementary material). Occasional monazite grains and apatite cements were present. The 1066.0 m Precipice Sandstone mudstone contained rutile and barite cements, zircon, and coal dispersed in a clay rich matrix (Figure 8C, D, and Supplementary material). This sample had a relatively low porosity measured by QEMSCAN of 1.82%. Precipice Sandstone 1033.88 m contained coal layers and dispersed coal and siderite cements (Figure 8).

Intergranular porosity had generally been filled in the Evergreen Formation samples by calcite, siderite, or kaolinite cements with porosities of 0.69 – 1.63%. The 1020.89 m Evergreen Formation core section was fine grained and clay rich (Figure 9 and supplementary material). It contained coal layers and dispersed coal, with pyrite and barite cements associated with the coals (Figure 9, and supplementary material). Barite cement was also associated with etched K-feldspar grains. Rutile cements were occasionally associated with FeCu-sulphide cement. Pore filling siderite also occurred surrounding pore filling kaolinite. The Evergreen Formation 1024.23 m contained pore filling siderite, kaolinite and illite, with corroded K-feldspar and occasional rutile and zircon grains (Figure 9). Calcite, siderite, and kaolinite cemented pores in Evergreen Formation 1015.0 m (Figure 9 and supplementary material), this core also contained a relatively high K-feldspar content.

A wider range of 13 Tipton 153 well core depth sections were analysed for whole rock total metals (supplementary material). The total Sr content was an order of magnitude higher in the Evergreen Formation seal cores than in the Precipice Sandstone (supplementary material), or in any of the Southwood 1 cores (Table 3). The highest total concentrations of Mn were in the Precipice mudtone from 1067.92 m and the calcite and siderite cemented Evergreen core from 1015.00 m. The Precipice Sandstone mudstone from 1066.00 m depth contained the highest concentrations of Rb, Mg, Li, Pb, Zr, Cu, Cr, Th, Co, U, and Ni along with several other elements. The Evergreen mudstone from 1020.89 m also contained relatively elevated element concentrations.

A drill core from the basement Raceview Formation directly underlying the Precipice Sandstone was also sampled, this contained a fault section with coal layers, and below a siderite cemented shale with pyrite filled fractures (supplementary material).

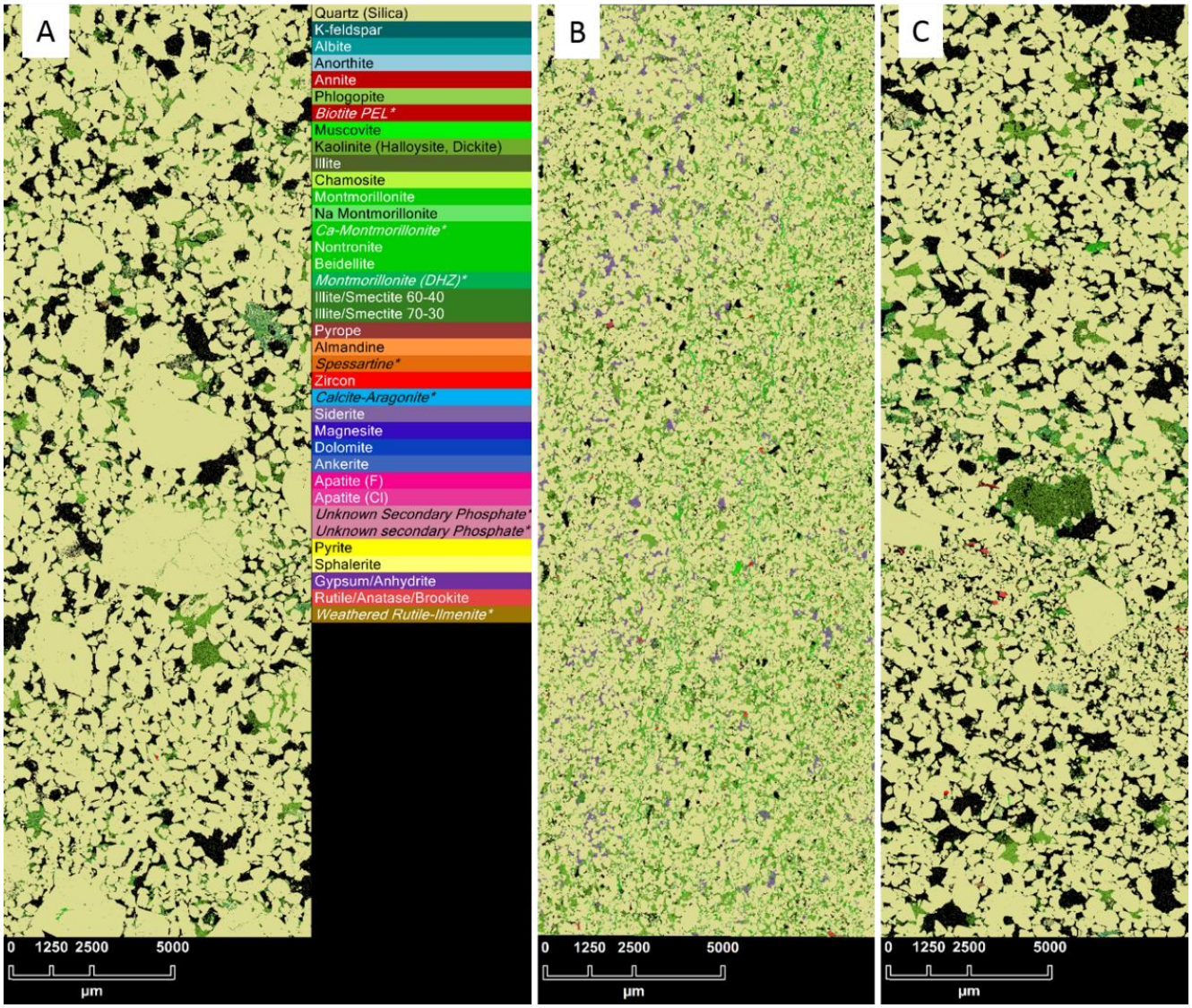

403

404 Figure 7: Tipton 153 well Precipice Sandstone QEMSCAN images. A) 1093.0 m with some
405 quartz grain fracturing, B) siderite cements in 1067.92 m note the bedding plane is in the
406 vertical direction in this image, C) 1032.25 m.

407

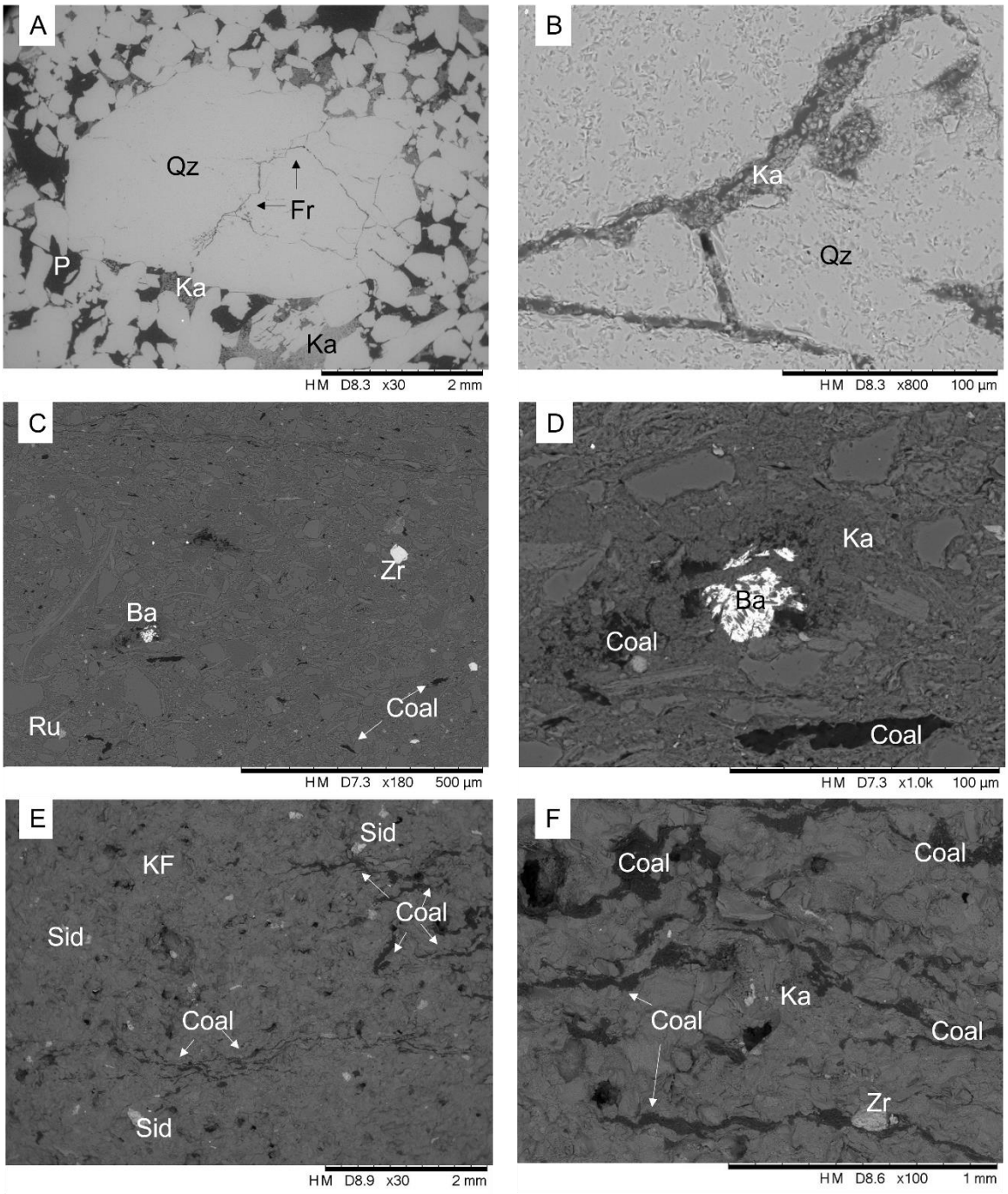

408

409 Figure 8: Tipton 153 well core SEM images of reservoir Precipice Sandstone. A) and B) 1093.0
410 m fractured quartz grains filled with kaolinite. C) and D) Precipice Sandstone 1066.0 m
411 mudstone layer with zircon, dispersed coal, barite and rutile cements in the clay matrix. E)
412 1033.88 m with coal layers, siderite cements and dispersed coal. F) 1033.88 m Coal layers,
413 kaolinite and zircon. Qz = quartz, Fr = fracture, Sid = siderite, Ka = kaolinite, KF = K-feldspar,
414 Zr = zircon, Ba = barite, Ru = rutile, and P = intergranular pore.

415

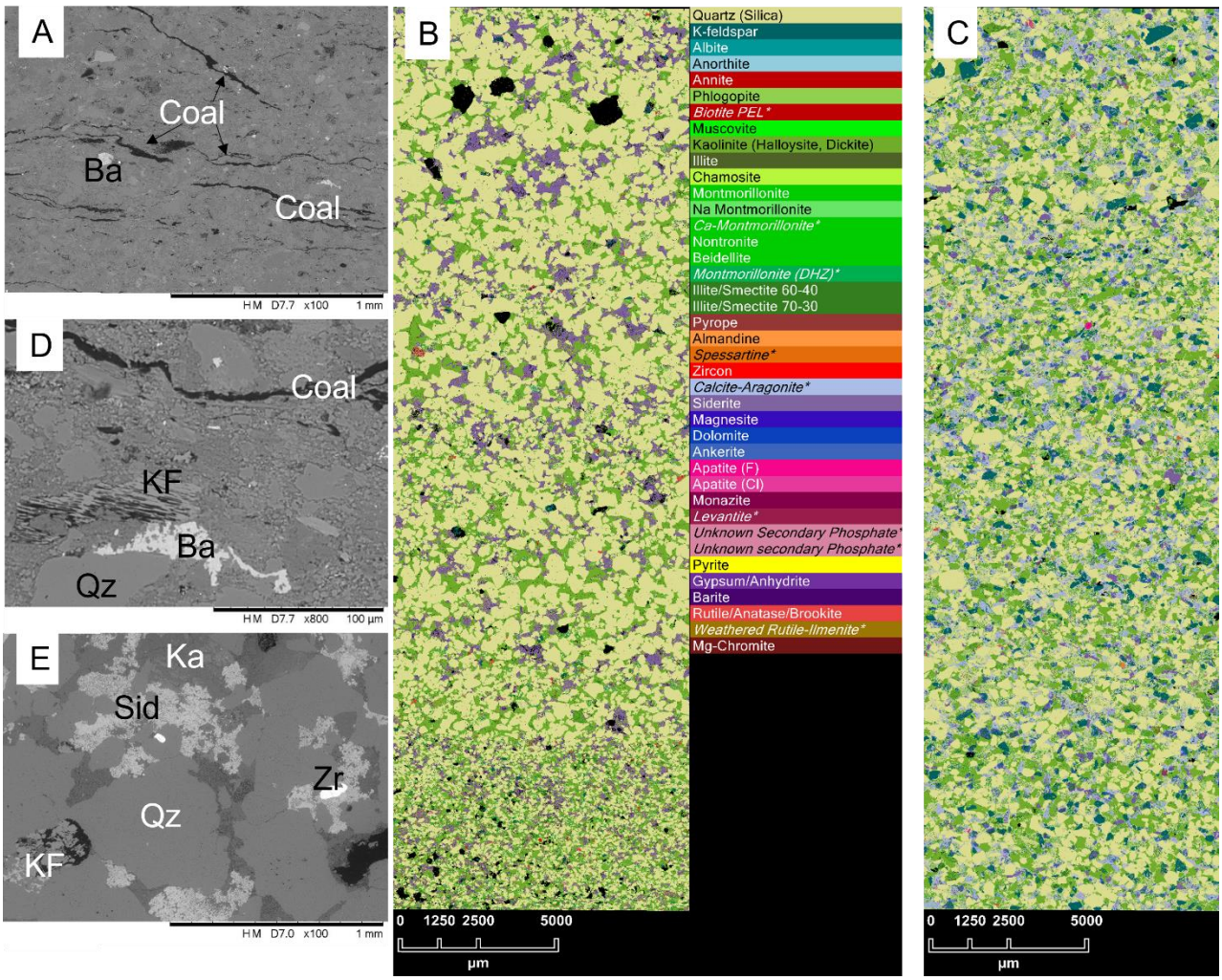

Figure 9: Tipton 153 well core SEM and QEMSCAN images from the Evergreen Formation seals. A) SEM image of 1020.89 m with coal layers and barite cement. B) QEMSCAN image of Siderite cemented 1024.23 m. C) QEMSCAN image of calcite and siderite cemented 1015.0 m. D) SEM image of 1020.89 m with coal layers, and barite cement associate with corroded K-feldspar. E) SEM image of 1024.23 m with corroded K-feldspar, pore filling kaolinite and siderite cements surrounding compacted quartz grains and zircon grains. Qz = quartz, Sid = siderite, Ka = kaolinite, KF = K-feldspar, Zr = zircon, and Ba = barite. Additional mudstone core depth sections are shown in supplementary material.

3.2 Synchrotron XFM

Southwood 1 well

Figure 10 shows XFM scans of the Precipice Sandstone core from Southwood 1 1994.13 m displayed as concentration of Rb (top), and Fe (bottom). SEM images of the same areas are

also shown. Rb was present in the k-feldspar, including the grains that had undergone previous corrosion, Rb was also present in pore filling illite. XFM images of K in K-feldspar and illite are also shown in the supplementary material. Fe and Mn were mainly in pore filling siderite (Figure 10, 11). Sr was occasionally observed in siderite and also occasionally in K-feldspar. Distributions of Ti and Zr are shown in supplementary material where they were mainly present in rutile cements and zircon grains. Pb was mainly in fine grained pyrite cement and FeZn sulphides. Zn was present in fine grained FeZn sulphides that generally rimmed pore filling siderites (supplementary material).

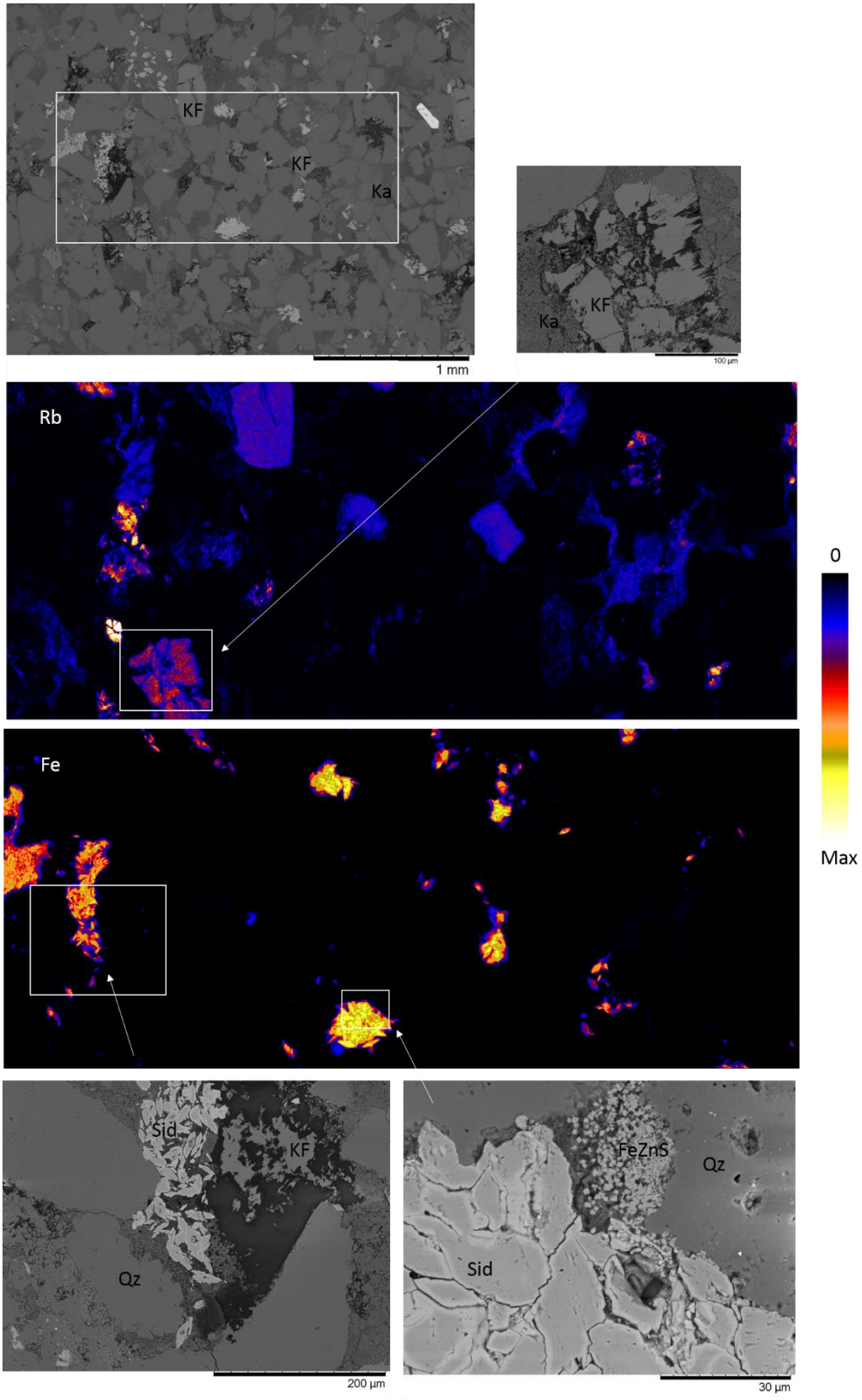

438

439 Figure 10: XFM images of Southwood 1 Precipice Sandstone 1994.13 m with concentration

440 of Rb in top image and Fe below. The maximum concentration shown of Rb = 0.167%, and

441 Fe = 83.2%. Associated SEM images of the XFM area, corroded K-feldspar, and siderite
442 (clockwise) are also shown. Sid = siderite, Qz = quartz, Ka = kaolinite, KF = K-feldspar, FeZnS =
443 FeZn sulphide cement. Further images are shown in supplementary material.

444

445

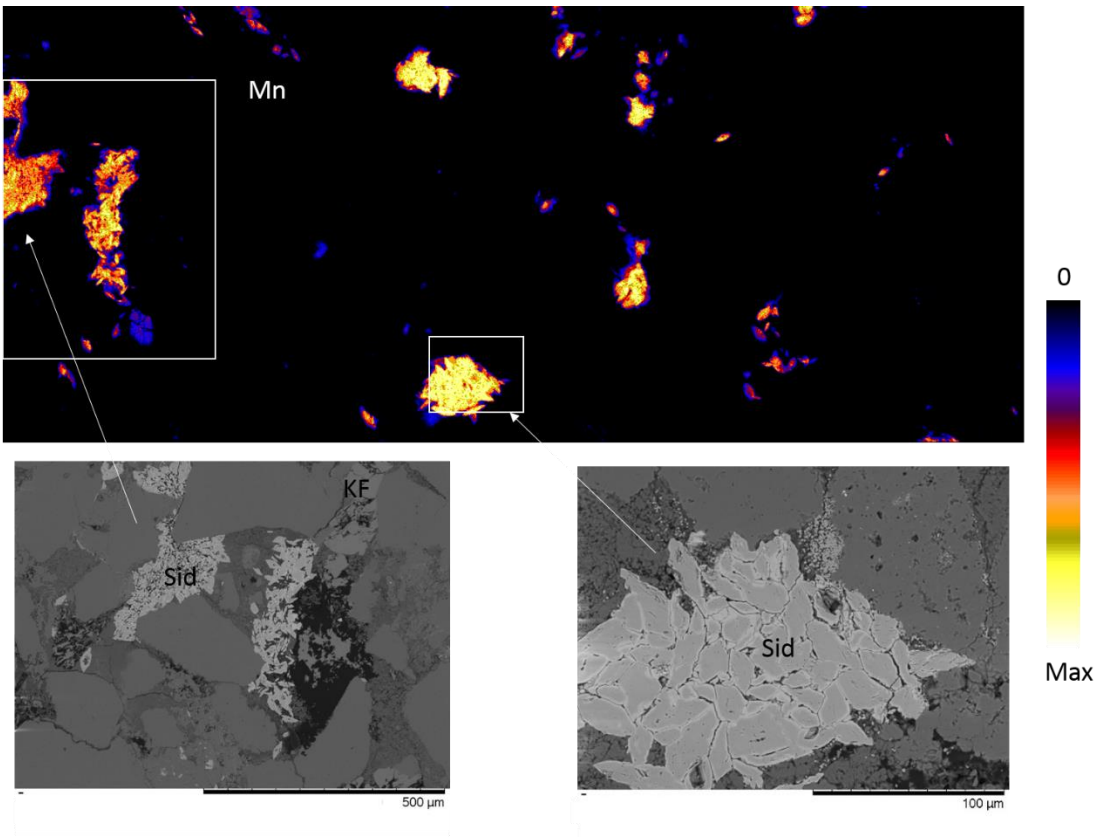

446

447 Figure 11: XFM images of Southwood 1 Precipice Sandstone 1994.13 m with concentration
448 of Mn. The maximum concentration shown of Mn = 2.90%. Associated SEM images are also
449 shown of siderite areas. Sid = siderite, Qz = quartz, KF = K-feldspar.

450

451 **Tipton 153 well**

452 Two Tipton 153 samples from the Precipice Sandstone at 1067.92 m, and the Evergreen
453 Formation at 1015.00 m were scanned in XFM. Mn was hosted in siderite and Rb in both
454 muscovite and K-feldspar in the 1067.92 m core (Figures 12, 13). Sr, Th and Pb were
455 present in occasional monazite grains (supplementary material). In the calcite cemented
456 Evergreen Formation core 1015.00 m, Mn was mainly hosted in siderite, and also present in

457 calcite. Sr was mainly in calcite, and occasional apatite cement and mixed phosphate
458 containing cements, and K-feldspar, with Rb again hosted in K-feldspar (Figures 14, 15).

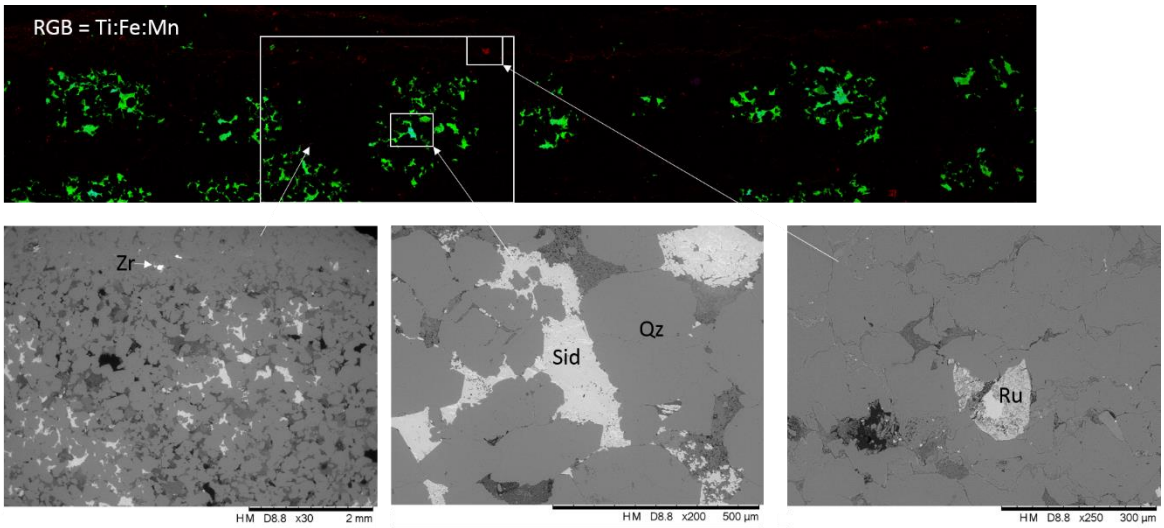

459

460 Figure 12: XFM image of part of Tipton 153 Precipice Sandstone 1067.92 m. Red:Green:Blue
461 = Ti:Fe:Mn. Maximum concentrations shown are Ti 64.88%, Fe 58.66%, Mn 3.83%. SEM
462 images of zircon (Zr), siderite (Sid) cement and rutile (Ru) cement in compacted quartz (Qz)
463 are also shown.

464

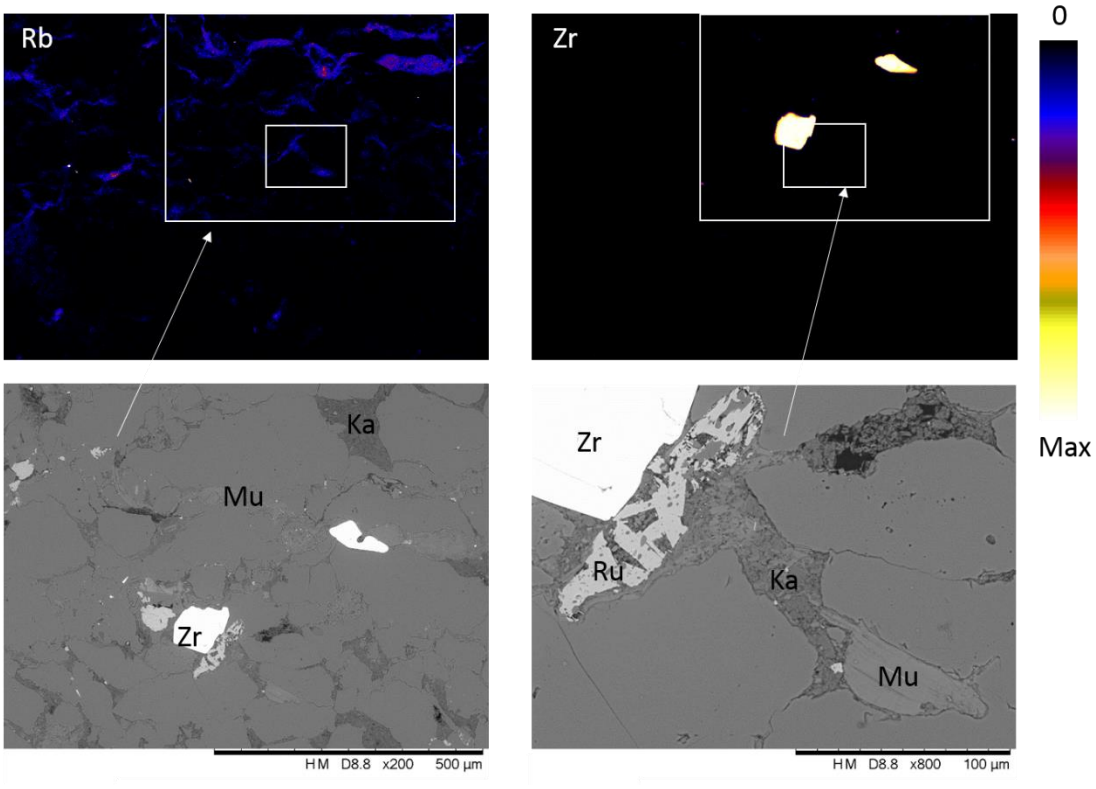

465

Figure 13: XFM images of Tipton 153 Precipice Sandstone 1067.92 m shown as concentrations of Rb (maximum concentration 0.1%) and Zr (maximum concentration 21.57%). SEM images of boxed areas with zircon (Zr), muscovite layers (Mu), kaolinite (Ka), and rutile (Ru) cement are also shown.

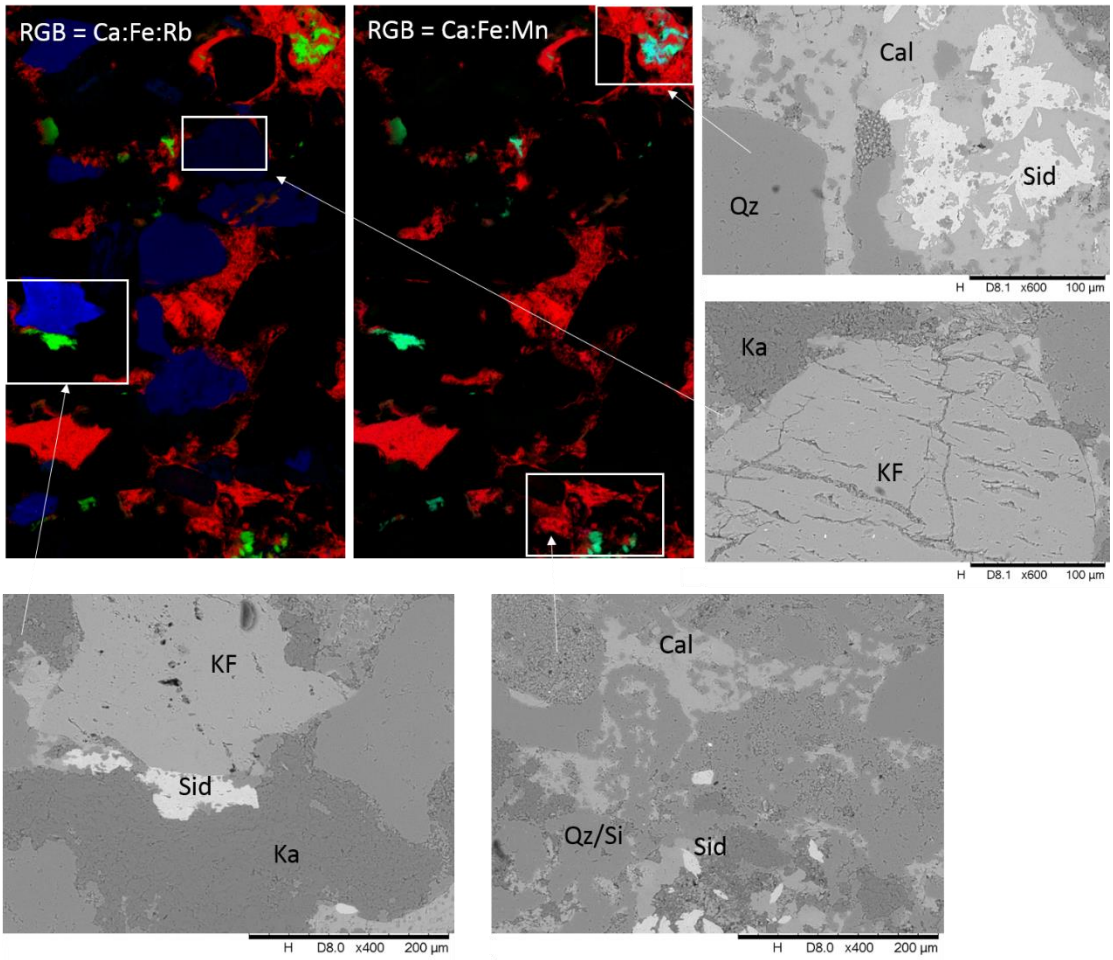

Figure 14: XFM image of Tipton 153 Evergreen Formation 1015.0 m. Red:Green:Blue = Ca:Fe:Rb and Ca:Fe:Mn. Maximum concentrations in the images are Ca = 60.28%, Fe = 55.50%, Rb = 0.17%, Mn = 2.95%. SEM images of boxed areas are also shown with calcite (Cal) and siderite (Sid) cements, pore filling kaolinite (Ka), quartz (Qz), K-feldspar (KF), and quartz or silica cement (Qz/Si).

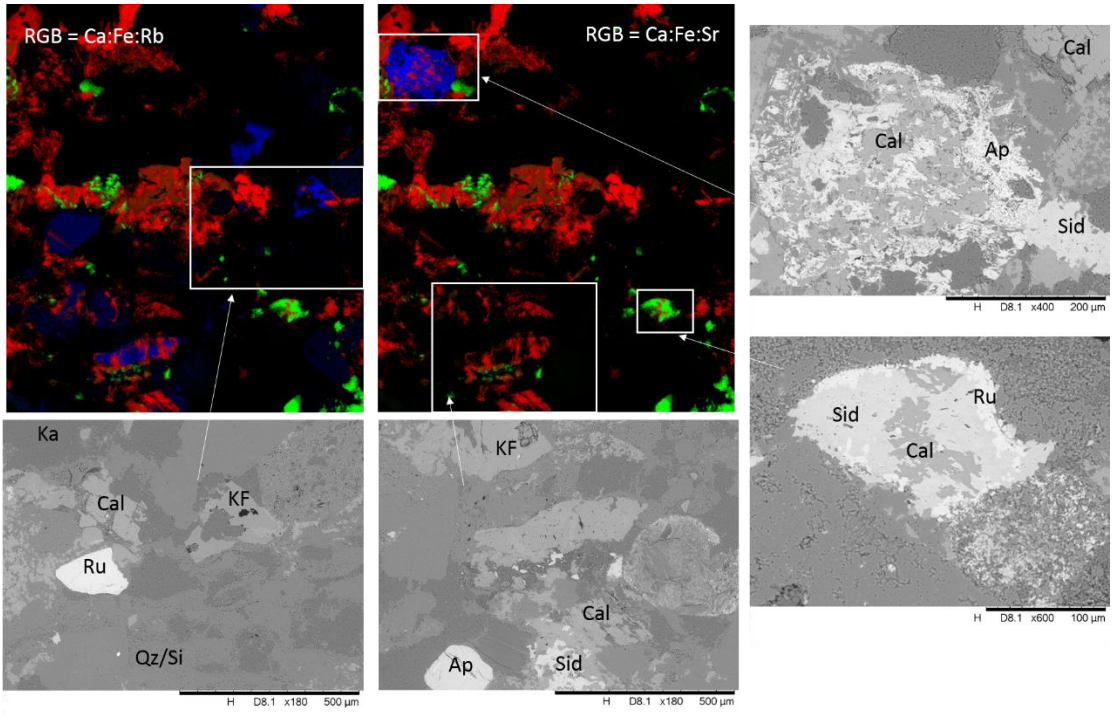

478

479 Figure 15: XFM images of a second area in Tipton 153 Evergreen Formation 1015.0 m.
480 Red:Green:Blue = Ca:Fe:Rb and Ca:Fe:Sr. Maximum concentrations in the images are Ca =
481 64.39%, Fe = 57.30%, Rb = 958.1 ppm, Sr = 6.67%. SEM images of boxed areas are also
482 shown with calcite (Cal), siderite (Sid), and apatite (Ap) cements, pore filling kaolinite (Ka), K-
483 feldspar (KF), quartz or silica cement (Qz/Si), and rutile (Ru).

484

485 **3.3 Kinetic geochemical modelling**

486 Geochemical models were run for the reaction of dissolved CO_2 with two Precipice
487 Sandstone sample compositions from the Southwood 1 well and two from the Tipton 153
488 well over 30 and 1000 years. One Evergreen Formation sample from the Southwood 1 well,
489 and one from the Tipton 153 well were also run. A total of twenty models are summarised
490 in Table 4.

491

492 Table 4: Summary of models run with predicted pH and mineral trapping where calculated.
493 The input parameters including water chemistries and mineral reactive surface areas (SA)
494 are given in detail in the supplementary material.

Formation and allocation	Well	Depth (m)	Time (y)	CO_2 fugacity	Water chemistry	Mineral SA	End pH	mineral trapping

								(kg CO_2 /m^3)
Precipice Reservoir	Southwood 1	1994.13	30	Full	1	Full	4.57	0.095 siderite
Precipice Reservoir	Southwood 1	1993.47	30	Full	1	Full	4.38	-0.006
Evergreen seals	Southwood 1	1952.85	30	Full	1	Full	4.52	0.001 siderite
Precipice Reservoir	Southwood 1	1994.13	1000	Full	1	Full	5.14	1.24 siderite
Precipice Reservoir	Southwood 1	1993.47	1000	Full	1	Full	4.8	-0.02
Evergreen seals	Southwood 1	1952.85	1000	Full	1	Full	4.94	0.044 siderite
Precipice Reservoir	Southwood 1	1994.13	1000	Half	1	Full	5.43	
Precipice Reservoir	Southwood 1	1993.47	1000	Half	1	Full	5.0	
Evergreen seals	Southwood 1	1952.85	1000	Half	1	Full	5.2	
Precipice Reservoir	Southwood 1	1993.47	1000	Full	1	10x lower	4.5	
Precipice Reservoir	Southwood 1	1993.47	1000	Full	1a	Full	4.51	
Evergreen Seals	Southwood 1	1952.85	1000	Full	1a	Full	4.58	
Precipice Reservoir	Tipton 153	1093.00	30	Full	2	Full	4.56	0.034 siderite
Precipice Reservoir	Tipton 153	1067.92	30	Full	2	Full	4.7	0.069 siderite
Evergreen Seals	Tipton 153	1015.00	30	Full	2	Full	4.93	0.244 ankerite
Precipice Reservoir	Tipton 153	1093.00	1000	Full	2	Full	5.03	0.58 siderite
Precipice Reservoir	Tipton 153	1067.92	1000	Full	2	Full	5.32	1.43 siderite
Evergreen Seals	Tipton 153	1015.00	1000	Full	2	Full	5.2	2.6 ankerite
Precipice Reservoir	Tipton 153	1067.92	1000	Full	2	10x lower	4.88	
Evergreen Seals	Tipton 153	1015.00	1000	Full	2	10x lower	4.99	

Southwood 1 well

Kinetic geochemical models were run for CO_2 reactions of three Southwood 1 well cores: Precipice Sandstone 1994.13 m containing siderite and feldspar, quartz rich Precipice Sandstone 1993.47 m, and Evergreen Formation 1952.85 m containing siderite and feldspar.

The predicted change in minerals and pH over 30 years are shown in Figure 16 for 1994.13 m. In the reaction of Southwood 1 1994.13 m Precipice Sandstone, siderite was predicted to dissolve and reprecipitate, with Fe-rich chlorite altered to additional siderite. K-feldspar, albite and smectite were altered to smectite, chalcedony and kaolinite (Figure 16a). Overall, only 0.095 kg/m^3 of CO_2 was predicted to be mineral trapped as siderite after 30 years. The

505 predicted pH decreased from 6.72 to 4.23 on addition of CO_2. After 30 years the pH was
506 4.57 (Table 4, and supplementary material), and after 1000 years 5.14 (Figure 16b). After
507 1000 y 1.24 kg/m^3 of CO_2 was predicted to be mineral trapped as siderite.

508 The CO_2 reactivity of quartz rich Precipice Sandstone Southwood 1 1993.47 m was predicted
509 to be relatively low, resulting in the pH remaining relatively low at 4.38 after 30 years (Table
510 4 and supplementary material), and after 1000 years 4.8 (Figure 16 C,D). Kaolinite and
511 chalcedony were precipitated from the alteration of feldspars. Overall dissolution of siderite
512 resulted in a net negative mineral trapping of - 0.006 and - 0.02 kg/m^3 of CO_2 after 30 and
513 1000 y respectively. This sample was also run with lower mineral reactive surface areas (10
514 times lower than the base case), with the pH lower at 4.5 after 1000 years (supplementary
515 material).

516 In the reaction of the Southwood 1 Evergreen Formation 1952.85 m, feldspars were altered
517 to kaolinite and chalcedony, and the pH was 4.52 after 30 years (Table 4 and supplementary
518 material) and 4.94 after 1000 y (Figure 16 E, F). Precipitation of siderite trapped only 0.001
519 kg/m^3 of CO_2 after 30 y and 0.044 kg/m^3 after 1000 y.

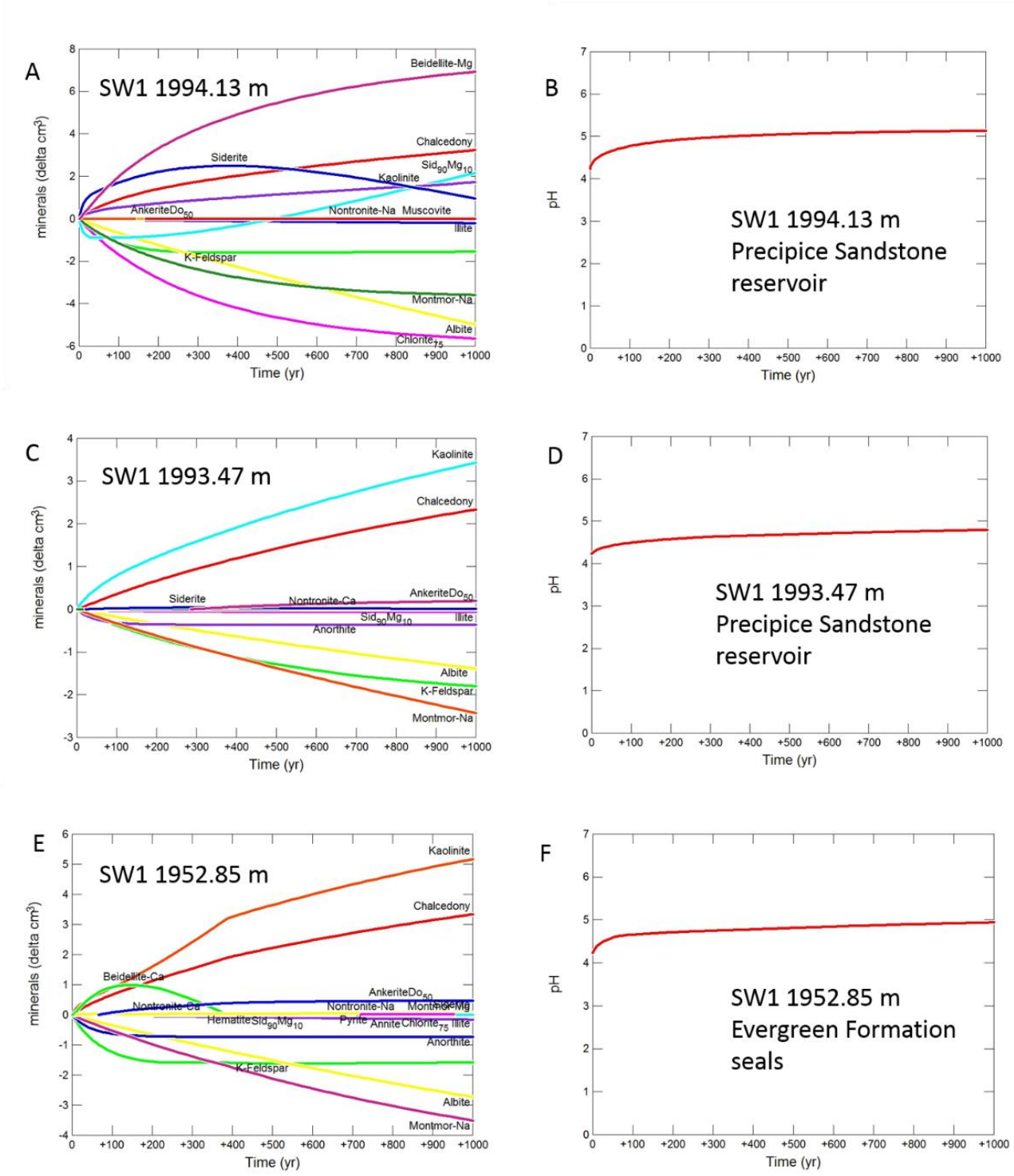

520

521 Figure 16: Kinetic geochemical models of dissolved CO_2 – formation water reactions of
522 Southwood 1 well core over 1000 years. A) and B) Precipice Sandstone 1994.13 m containing
523 siderite and feldspar, showing predicted change in minerals and pH. C) and D) quartz rich
524 Precipice Sandstone 1993.47 m predicted change in minerals and pH. E) and F) Evergreen
525 Formation 1952.85 m containing siderite and feldspar, predicted change in minerals and pH.

Models of the reactions of Southwood 1 Precipice Sandstones 1994.13m, 1993.47 and Evergreen Formation 1952.85 m were also run over 1000 years with lower CO_2 fugacities (half of the base case) to simulate plume edges or regions of depleted CO_2. They predicted the precipitation of lower mineral volumes, with the predicted formation water pH higher at 5.43, 5.0 and 5.2 for 1994.13 m, 1993.47 m and 1952.85 m respectively (Table 4 and supplementary material). Separate reactions of Southwood 1 1993.47 m and 1952.85 m were also run over 30 years with CO_2 and a sodium bicarbonate character groundwater resulting in predicted pH of 4.51 and 4.58 respectively (only slightly higher than the base case with the sodium chloride character groundwater) (supplementary material). The changes in mineral content were otherwise very similar.

Tipton 153 well

Kinetic geochemical models were run over 30 and 1000 y for the calcite cemented Evergreen Formation Tipton 153 1015.00 m, the Precipice Sandstone containing siderite cement from 1067.92 m, and the quartz rich Precipice Sandstone at 1093.00 m (Table 4, Figure 17, and supplementary material).

On reaction of the Evergreen Formation Tipton 153 1015.00 m with CO_2, the pH decreased from 6.50 to 4.48. Calcite dissolved and reprecipitated increasing pH rapidly, with the pH 4.93 after 30 years and 5.2 after 1000 years. Plagioclase, siderite and K-feldspar also dissolved with kaolinite, siderite, smectite, ankerite and chalcedony mainly precipitating (Figure 17A,B, and supplementary material). After 30 y 0.244 kg/m^3 of CO_2 was predicted to be mineral trapped as ankerite and calcite, after 1000 y 2.6 kg/m^3 of CO_2 was mineral trapped as ankerite.

The Precipice Sandstone Tipton 153 1067.92 m underwent slight dissolution and subsequent reprecipitation of siderite, with additional alteration of chlorite to siderite (Figure 17 C,D, and supplementary Material). Smectite and albite also altered to kaolinite, smectite and chalcedony. The pH was 4.7 after 30 y and 5.32 after 1000 y. Overall CO_2 was mineral trapped as siderite with 0.069 kg/m^3 CO_2 after 30 y and 1.43 kg/m^3 CO_2 trapped after 1000 y.

The Precipice Sandstone from 1093.00 m was predicted to be less reactive with traces of chlorite, smectite, and albite converted to kaolinite, siderite and chalcedony. With the pH 4.56 after 30 years (Table 4 and supplementary material), and 5.03 after 1000 years (Figure 17 E,F). Overall siderite precipitation resulted in 0.034 kg/m^3 CO_2 mineral trapped after 30

558 years. After 1000 y mainly siderite precipitation with a trace of ankerite precipitation
559 mineral trapped 0.58 kg/m^3 of CO_2.

560 Tipton 153 calcite cemented Evergreen Formation 1015.0 m, and siderite cemented
561 Precipice Sandstone 1067.92 m were also run over 1000 years with mineral reactive surface
562 areas 10 times lower than the base case. After 1000 years the pH was predicted to be 4.99
563 and 4.88 for 1015.0 and 1067.92 m respectively, only slightly lower than for the base cases
564 (at 5.2 and 5.3 respectively) (supplementary material).

565

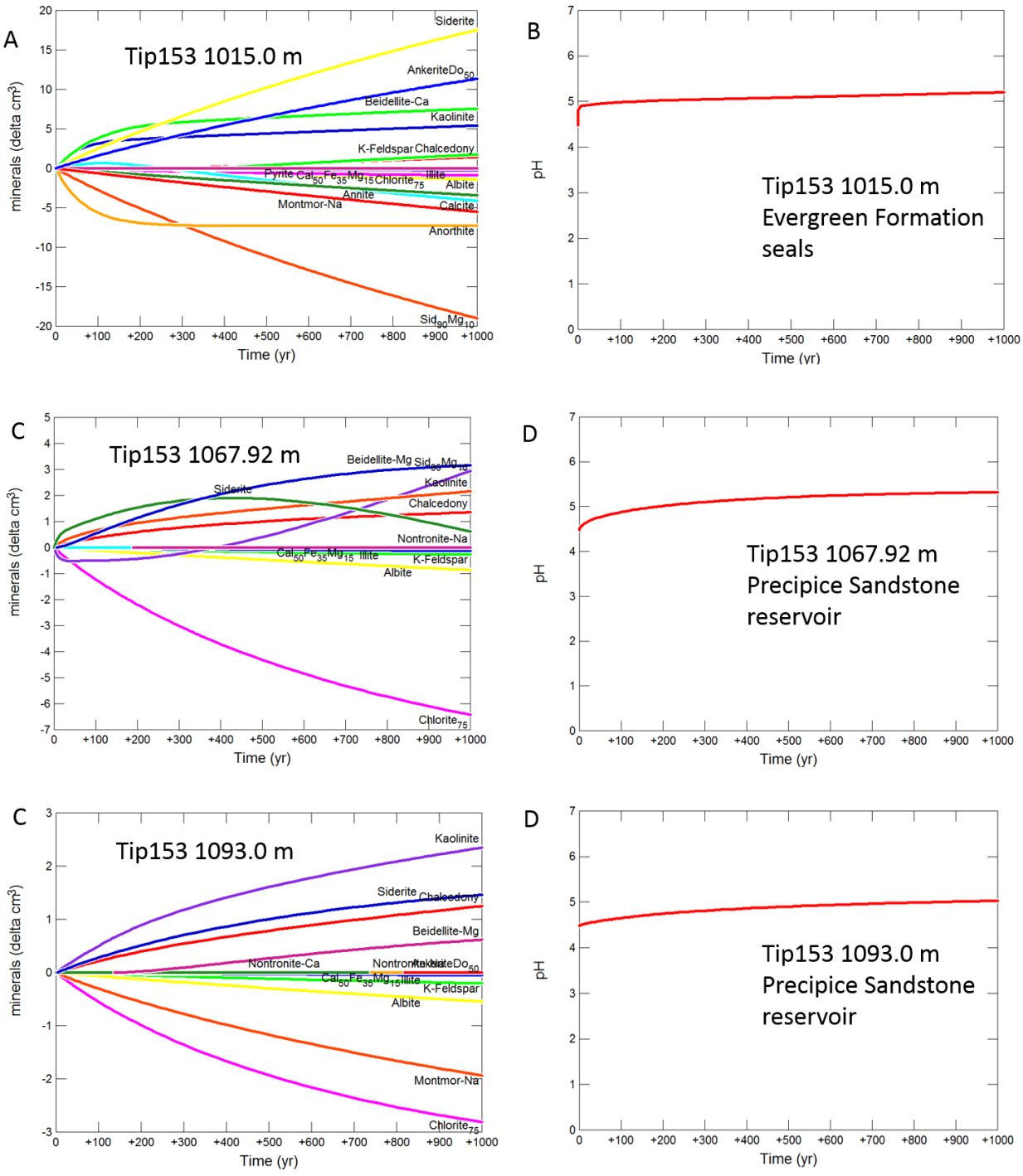

566

567 Figure 17: Kinetic geochemical models of dissolved CO_2 – formation water reactions of
568 Tipton 153 well core over 1000 years, predicted change in minerals and pH. A) and B)
569 Calcite and siderite cemented Evergreen Formation 1015.00 m, C) and D) siderite cemented
570 Precipice Sandstone 1067.92 m, E) and F) quartz rich Precipice Sandstone 1093.00 m.

571

4. Discussion

The southern Surat Basin is undergoing feasibility studies for industrial CO_2 storage. Reservoir and seal units from the Precipice Sandstone and Evergreen Formation of two well cores in the southern Surat were characterised and their long term geochemical reactivity to CO_2 predicted. Quartz rich reservoir sandstones (Precipice Sandstone) had higher porosities, lower mecury injection threshold pressures, and showed low reactivity to CO_2 relative to the Evergreen Formation. This is likely to be favourable for CO_2 injection. Siderite was present in the Precipice Sandstone in both wells along with kaolinite. Natural fractures, quartz grain fracturing, and alteration were present in several core depths, especially in the Southwood 1 well located near a fault zone. The interbedded nature of reservoirs, seals and thin coal layers, with cements and grain compaction will likely baffle CO_2 fluids reducing vertical migration. The effect of these and quartz grain fracturing on migration of the CO_2 could be investigated in future in experimental core flooding and dynamic models. The Southwood 1 well overall contained more fracturing of quartz grains and grain compaction likely owing to its proximity to the Moonie Goondiwindi fault zone (He et al., 2021). The two quartz rich Precipice Sandstones, Southwood 1 1993.47 m and Tipton 153 1093 m, had overall low reactivity with predicted dissolution of siderite on reaction with CO_2 and slightly negative mineral trapping. Siderite cemented and feldspar containing sandstones from the Precipice Sandstone were predicted to undergo K-feldspar alteration to kaolinite, with chlorite and plagioclase alteration to siderite or ankerite with 0.02 to 1.43 kg/m^3 CO_2 trapped after 1000 years. Existing siderite and calcite cements in an Evergreen Formation core initially dissolved, buffering pH. Plagioclase was converted to ankerite trapping up to 2.6 kg/m^3 CO_2 after 1000 years. Studies in the shallower low salinity north region of the Surat Basin predicted no mineral trapping in the reservoir, with 0.03 to 8.4 kg/m^3 CO_2 trapped in seals (Pearce et al., 2021; Pearce et al., 2020). Mineral trapping in reservoir sandstones of the Upper Silesian Coal Basin, Central Europe, was also low at 1 - 2 kg/m^3 CO_2 (Labus and Bujok, 2011). Predicted mineral trapping of 90 kg/m^3 was reported in Gulf Coast interbedded sandstone and shale over 100,000 years as dawsonite, ankerite and siderite (Xu et al., 2005). Oligoclase (plagioclase) and chlorite were the main minerals providing ions for mineral trapping along with Fe-oxide. Natural mineral trapping over geological timescales has been estimated at 34 and 232 kg/m^3 CO_2 in a reservoir and overlying formation of the Otway Basin, Australia. Although over longer time scales than the current study, the higher magnitude of mineral trapping in clay rich seals than in reservoir rocks is in agreement. Mineral trapping as pore throat diameters in Precipice Sandstone core from the north of the

606 Surat Basin are generally sharp unimodal distributions around 100 µm (Pearce et al., 2019b;
607 Pearce et al., 2020). Those measured in this study from Southwood 1 core however have
608 broad distributions. Further MIP data of reservoir core and also seals is needed from the
609 South Surat to understand if this is representative of the region or due to a small sample set.
610 Variable reported permeabilities indicate higher permeability sections up to 219 mD may be
611 partly fracture controlled. The fracturing of quartz grains may be important for migration
612 studies if CO_2 is injected. History matching of the migration of the CO_2 at the Sleipner
613 injection site in Norway for example required the inclusion of natural fractures in
614 intraformational shale barriers to match the distance of migration (Cavanagh and
615 Haszeldine, 2014).

616 Signs of fractures, weathering or potential hydrothermal fluid or natural CO_2 alteration were
617 observed in both well cores, especially from Southwood 1 with highly altered feldspars
618 cemented with siderite, silica cements and veins, and delicate rutile, barite and apatite
619 cements. Predicted CO_2 alteration included calcite and siderite dissolution and
620 reprecipitation, K-feldspar alteration to kaolinite and silica, plagioclase conversion to
621 ankerite or smectite, and chlorite (or biotite) alteration to siderite. These are consistent
622 with reported alteration of formations exposed to natural accumulations of CO_2 such as
623 those containing chlorite and plagioclase (Higgs et al., 2013; Watson et al., 2004), natural or
624 experimental alteration of K-feldspar (Luquot et al., 2016; Pauwels et al., 2007; Yuan et al.,
625 2019), or reported predictions for CO_2 storage sites (Gherardi et al., 2007; Xu et al., 2005).
626 Overall CO_2 mineral trapping as the carbonates siderite and ankerite are mainly likely to also
627 re trap liberated Mn, Mg, Fe, Ca, Sr. K-feldspar dissolution may release Rb to solution over
628 longer time scales, this could allow monitoring of alteration via Sr isotopes of formation
629 water during CO_2 field injection. Further work with experimental CO_2 water rock reactions
630 and sequential extraction studies would be needed in future to understand site specific
631 release or sequestration of metals and to build and validate models (Kirste et al., 2017;
632 Kirste et al., 2019; Marcon and Kaszuba, 2015). Where studies in a site of the north Surat
633 Basin predicted any metal release would be limited to the CO_2 plume extent. Models
634 predictions in the current study could be improved through experimental CO_2-water-rock
635 reaction studies to parameterise and validate model reactive surface areas. The current
636 study also assumes a pure injected CO_2 stream. If a CO_2 "hub" approach, injecting CO_2 from
637 multiple industrial sources is employed, the CO_2 stream may contain different
638 concentrations and types of impurity or ancillary gases. Several, for example H_2S
639 (associated with natural gas), SOx and NOx (associated with coal combustion or cement and

steel production), or O_2 (associated with oxyfuel combustion or likely DAC) can have higher reactivity to rock that pure CO_2. Further experimental and modelling studies of reservoir and seal core or pilot injection tests should therefore assess a range of possible gas compositions.

5. Conclusions

- The Precipice Sandstone in the southern Surat Basin is undergoing feasibility studies as a reservoir for geological CO_2 storage. Reservoir and seal cores from two wells near the Moonie Goondiwindi fault zone and east towards the Clarence Morton Basin were characterised.
- Reservoir core was mainly quartz rich with open porosity indicating good reservoir potential and had quartz grain fracturing. MIP porosities range from 9 – 21%, and QEMSCAN open porosity from 4 – 22% and 2 – 17% with lower porosities associated with a mudstone layer. Seal cores were variable and included sandstones, carbonate cemented sandstone, and mudstone or shale containing coal layers. Seal porosities ranged from 1 – 19%.
- The majority of Mn was hosted in siderite, and Sr in calcite and apatite cements. Occasional monazite grains hosted Th and Pb; with Zn and As in sulphides. Rb was mainly hosted in muscovite and K-feldspar that is predicted to react in the long term.
- Reaction of mainly feldspars and chlorite were predicted with precipitation of kaolinite, chalcedony, calcite and smectite. Mineral trapping of up to 1.4 kg/m^3 of CO_2 as precipitated siderite was predicted in the reservoir after 1000 years. Mineral trapping was greater in the overlying seal at up to 2.6 kg/m^3 of CO_2 trapped as ankerite after 1000 years.

Declaration of competing interest

The authors declare no known competing interests.

Supplementary Material

Supplementary material is available for this article including a document containing additional data and images, two excel spreadsheets of mineral components, and an excel spreadsheet of whole rock element contents.

Acknowledgments

Part of this work was funded by the UQ Surat Deep Aquifer Appraisal Project (UQ-SDAAP). For their contribution and support, UQ would like to acknowledge: the Commonwealth Government of Australia Carbon Capture and Storage RD&D programme and ACA Low Emissions Technology Pty Ltd (ACALET). The information, opinions and views expressed here do not necessarily represent those of The University of Queensland, the Australian Government or ACALET. Researchers within or working with the UQ-SDAAP are bound by the same policies and procedures as other researchers within The University of Queensland, which are designed to ensure the integrity of research. The whole UQ-SDAAP team is thanked. A. Garnett and H. Schultz are acknowledged for funding support and internally reviewing the manuscript. Part of this work was funded by ANLEC R&D. The authors wish to acknowledge financial assistance provided through Australian National Low Emissions Coal Research and Development. ANLEC R&D is supported by Low Emission Technology Australia (LETA) and the Australian Government through the Department of Industry, Science, Energy and Resources.

Part of this research was undertaken on the XFM beamline at the Australian Synchrotron, ANSTO. This relates to grant no. AS183/XFM/13906 “Natural mineral trapping of regulated metals from groundwater by long term CO_2-fluid-rock interactions”. We acknowledge travel funding provided by the International Synchrotron Access Program (ISAP) managed by the Australian Synchrotron, part of ANSTO, and funded by the Australian Government. Ric Daniels of the Adelaide School of Petroleum, University of Adelaide, is thanked for performing MIP analyses. The UQ School of Earth and Environmental Sciences Environmental Geochemistry laboratory is thanked for whole performing rock element analyses. Dirk Kirste provided mineral script files for geochemical models. The staff of the GSQ Data Exploration Centre are thanked for access to drill core.

References

Bachu, S., Gunter, W.D., Perkins, E.H., 1994. AQUIFER DISPOSAL OF CO2 - HYDRODYNAMIC AND MINERAL TRAPPING. Energy Conv. Manag. 35, 269-279.
Bachu, S., Haug, K., 2005. In Situ Characteristics of Acid-Gas Injection Operations in the Alberta Basin, Western Canada: Demonstration of CO2 Geological Storage, Carbon Dioxide Capture for Storage in Deep Geologic Formations. Elsevier Science, Amsterdam, pp. 867-876.
Baublys, K.A., Hofmann, H., Esterle, J.S., Cendón, D.I., Vink, S., Golding, S.D., 2021. Geochemical influences on methanogenic groundwater from a low rank coal seam gas reservoir: Walloon Subgroup, Surat Basin. International Journal of Coal Geology 246, 103841.
Bethke, C.M., Yeakel, S., 2012. The Geochemist's Workbench (Version 9.0): Reaction modeling guide, 96 p ed. Aqueous Solutions, LLC, Champaign, Ill., 96 p.
Bianchi, V., Zhou, F., Pistellato, D., Martin, M., Boccardo, S., Esterle, J., 2018. Mapping a coastal transition in braided systems: an example from the Precipice Sandstone, Surat Basin. Australian Journal of Earth Sciences, 1-20.
Bickle, M., Kampman, N., Chapman, H., Ballentine, C., Dubacq, B., Galy, A., Sirikitputtisak, T., Warr, O., Wigley, M., Zhou, Z., 2017. Rapid reactions between CO2, brine and silicate minerals during geological carbon storage: Modelling based on a field CO2 injection experiment. Chem. Geol. 468, 17-31.
Bickle, M.J., Kampman, N., Wigley, M., 2013. Natural analogues, Geochemistry of Geologic Carbon Sequestration, Chapter in Reviews in Mineralogy and Geochemistry, pp. 15-71.
Busch, A., Amann-Hildenbrand, A., Bertier, P., Waschbuesch, M., Krooss, B.M., 2010. The Significance of Caprock Sealing Integrity for CO2 Storage, SPE International Conference on CO2 Capture, Storage, and Utilization,. Society of Petroleum Engineers, New Orleans, pp. SPE-139588-MS.
Carroll, S.A., McNab, W.W., Dai, Z., Torres, S.C., 2013. Reactivity of Mount Simon sandstone and the Eau Claire shale under CO2 storage conditions. Environmental Science and Technology 47, 252-261.
Cavanagh, A.J., Haszeldine, R.S., 2014. The Sleipner storage site: Capillary flow modeling of a layered CO2 plume requires fractured shale barriers within the Utsira Formation. Int. J. Greenh. Gas Control 21, 101-112.
Delany, J.M., Lundeen, S.R., 1989. The LLNL thermodynamic database. Lawrence Livermore National Laboratory Report UCRL-21658.
Duan, Z., Sun, R., 2003. An improved model calculating CO2 solubility in pure water and aqueous NaCl solutions from 273 to 533 K and from 0 to 2000 bar. Chem. Geol. 193, 257-271.
Ellis, B., Fitts, J., Bromhal, G., McIntyre, D., Tappero, R., Peters, C., 2013. Dissolution-Driven Permeability Reduction of a Fractured Carbonate Caprock. Environmental Engineering Science 30, 187-193.
Farquhar, S.M., Pearce, J.K., Dawson, G.K.W., Golab, A., Kirste, D., Biddle, D., Golding, S.D., 2015. A fresh approach to investigating CO2 storage: Experimental CO2-water-rock interactions in a freshwater reservoir system. Chem. Geol. 399, 98-122.
Feitz, A.J., Ransley, T.R., Dunsmore, R., Kuske, T.J., Hodgkinson, J., Preda, M., Spulak, R., Dixon, O. & Draper, J., 2014. Geoscience Australia and Geological Survey of Queensland Surat and Bowen Basins Groundwater Surveys Hydrochemistry Dataset (2009-2011).
Förster, A., Schöner, R., Förster, H.J., Norden, B., Blaschke, A.W., Luckert, J., Beutler, G., Gaupp, R., Rhede, D., 2010. Reservoir characterization of a CO2 storage aquifer: The Upper Triassic Stuttgart Formation in the Northeast German Basin. Marine and Petroleum Geology 27, 2156-2172.
Gherardi, F., Xu, T.F., Pruess, K., 2007. Numerical modeling of self-limiting and self-enhancing caprock alteration induced by CO2 storage in a depleted gas reservoir. Chem. Geol. 244, 103-129.

754 Gibson-Poole, C.M., Svendsen, L., Underschultz, J., Watson, M.N., Ennis-King, J., van Ruth,
755 P.J., Nelson, E.J., Daniel, R.F., Cinar, Y., 2008. Site characterisation of a basin-scale CO2
756 geological storage system: Gippsland Basin, southeast Australia. Environ. Geol. 54, 1583-
757 1606.
758 Golab, A.N., Carr, P.F., Palamara, D.R., 2006. Influence of localised igneous activity on cleat
759 dawsonite formation in Late Permian coal measures, Upper Hunter Valley, Australia.
760 International Journal of Coal Geology 66, 296-304.
761 Golding, S.D., Dawson, G.K.W., Pearce, J.K., Farrajota, F., Mernagh, T., Boreham, C.J., Hall,
762 L.S., Palu, T.J., 2016. Authigenic Carbonates in the Great Artesian Basin as Natural Analogues
763 for Mineralisation Trapping. ANLEC Project 7-1011-0189, CO2CRC report for ANLEC R&D.
764 Golding, S.D., Uysal, I.T., Bolhar, R., Boreham, C.J., Dawson, G.K.W., Baublys, K.A., Esterle,
765 J.S., 2013. Carbon dioxide-rich coals of the Oaky Creek area, central Bowen Basin: a natural
766 analogue for carbon sequestration in coal systems. Australian Journal of Earth Sciences 60,
767 125-140.
768 Golding, S.D., Uysal, I.T., Boreham, C.J., Kirste, D., Baublys, K.A., Esterle, J.S., 2011.
769 Adsorption and mineral trapping dominate CO2 storage in coal systems. Energy Procedia 4,
770 3131-3138.
771 Grigorescu, M., 2011. Mineralogy of the north-eastern Bowen Basin and north-eastern Surat
772 Basin, Queensland. Queensland Geological Record.
773 Hamilton, J.L., Wilson, S.A., Morgan, B., Turvey, C.C., Paterson, D.J., Jowitt, S.M.,
774 McCutcheon, J., Southam, G., 2018. Fate of transition metals during passive carbonation of
775 ultramafic mine tailings via air capture with potential for metal resource recovery. Int. J.
776 Greenh. Gas Control 71, 155-167.
777 Hamilton, S.K., Golding, S.D., Esterle, J.S., Baublys, K.A., Ruyobya, B.B., 2020. Controls on Gas
778 Domains and Production Behaviour in A High-Rank CSG Reservoir: Insights from Molecular
779 and Isotopic Chemistry of Co-Produced Waters and Gases from the Bowen Basin, Australia.
780 Geosciences 10, 74.
781 He, J., La Croix, A.D., Gonzalez, S., Pearce, J., Ding, W., Underschultz, J.R., Garnett, A., 2021.
782 Quantifying and modelling the effects of pre-existing basement faults on folding of overlying
783 strata in the Surat Basin, Australia: Implications for fault seal potential. Journal of Petroleum
784 Science and Engineering 198, 108207.
785 He, J., La Croix, A.D., Wang, J., Ding, W., Underschultz, J.R., 2019. Using neural networks and
786 the Markov Chain approach for facies analysis and prediction from well logs in the Precipice
787 Sandstone and Evergreen Formation, Surat Basin, Australia. Marine and Petroleum Geology
788 101, 410-427.
789 Higgs, K.E., Funnell, R.H., Reyes, A.G., 2013. Changes in reservoir heterogeneity and quality
790 as a response to high partial pressures of CO2 in a gas reservoir, New Zealand. Marine and
791 Petroleum Geology 48, 293-322.
792 Higgs, K.E., Haese, R.R., Golding, S.D., Schacht, U., Watson, M., 2015. The Pretty Hill
793 Formation as a natural analogue for CO2 storage; an investigation of mineralogical and
794 isotopic changes associated with sandstones exposed to low, intermediate and high CO2
795 concentrations over geological time. Chem. Geol. 399, 36-64.
796 Hodgkinson, J., Grigorescu, M., 2012. Background research for selection of potential
797 geostorage targets—case studies from the Surat Basin, Queensland. Australian Journal of
798 Earth Sciences 60, 71-89.
799 Howard, D.L., de Jonge, M.D., Afshar, N., Ryan, C.G., Kirkham, R., Reinhardt, J., Kewish, C.M.,
800 McKinlay, J., Walsh, A., Divitcos, J., Basten, N., Adamson, L., Fiala, T., Sammut, L., Paterson,
801 D.J., 2020. The XFM beamline at the Australian Synchrotron. Journal of Synchrotron
802 Radiation 27, 1447-1458.
803 IEA, 2020. Direct Air Capture. IEA, Paris. https://www.iea.org/reports/direct-air-capture.

IPCC, 2005. IPCC special report on carbon dioxide capture and storage, in: Metz, B., Davidson, O., de Coninck H.C., Loos, M., Meyer, L.A. (Eds.) (Ed.). Working Group III of the Intergovernmental Panel on Climate Change, p. 442.
Johnson, G., Mayer, B., Shevalier, M., Nightingale, M., Hutcheon, I., 2011. Quantifying CO2 pore-space saturation at the Pembina Cardium CO2 Monitoring Pilot (Alberta, Canada) using oxygen isotopes of reservoir fluids and gases. Energy Procedia 4, 3942-3948.
Kaszuba, J.P., Navarre-Sitchler, A., Thyne, G., Chopping, C., Meuzelaar, T., 2011. Supercritical carbon dioxide and sulfur in the Madison Limestone: A natural analog in southwest Wyoming for geologic carbon-sulfur co-sequestration. Earth and Planetary Science Letters 309, 131-140.
Kharaka, Y.K., Abedini, A.A., Gans, K.D., Thordson, J.J., Beers, S.R., Thomas, R.B., 2018. Changes in the chemistry of groundwater reacted with CO2: Comparison of results from laboratory experiments and the ZERT field site, Bozeman, Montana, USA. Appl. Geochem. 98, 75-81.
Kharaka, Y.K., Cole, D.R., Hovorka, S.D., Gunter, W.D., Knauss, K.G., Freifeld, B.M., 2006. Gas-water-rock interactions in Frio Formation following CO2 injection: Implications for the storage of greenhouse gases in sedimentary basins. Geology 34, 577-580.
Kirste, D., Pearce, J., Golding, S., 2017. Parameterizing Geochemical Models: Do Kinetics of Calcite Matter? Procedia Earth and Planetary Science 17, 606-609.
Kirste, D., Pearce, J.K., Golding, S.D., Dawson, G.K.W., 2019. Trace element mobility during CO2 storage: application of reactive transport modelling. E3S Web Conf. 98, 04007.
Köhler, S.J., Dufaud, F., Oelkers, E.H., 2003. An experimental study of illite dissolution kinetics as a function of ph from 1.4 to 12.4 and temperature from 5 to 50°C. Geochimica et Cosmochimica Acta 67, 3583-3594.
La Croix, A.D., Wang, J., He, J., Hannaford, C., Bianchi, V., Esterle, J., Undershultz, J.R., 2019a. Widespread nearshore and shallow marine deposition within the Lower Jurassic Precipice Sandstone and Evergreen Formation in the Surat Basin, Australia. Marine and Petroleum Geology 109, 760-790.
La Croix, A.D., Wang, J., Underschultz, J., 2019b. Integrated facies analysis of the Precipice Sandstone and Evergreen Formation in the Surat Basin, The University of Queensland Surat Deep Aquifer Appraisal Project - supplementary detailed report. The University of Queensland.
Labus, K., Bujok, P., 2011. CO2 mineral sequestration mechanisms and capacity of saline aquifers of the Upper Silesian Coal Basin (Central Europe) - Modeling and experimental verification. Energy 36, 4974-4982.
Liu, D., Wall, T., Stanger, R., 2016. CO2 quality control in Oxy-fuel technology for CCS: SO2 removal by the caustic scrubber in Callide Oxy-fuel Project. Int. J. Greenh. Gas Control 51, 207-217.
Lowson, R.T., Brown, P.L., Comarmond, M.C.J., Rajaratnam, G., 2007. The kinetics of chlorite dissolution. Geochimica et Cosmochimica Acta 71, 1431-1447.
Luquot, L., Gouze, P., Niemi, A., Bensabat, J., Carrera, J., 2016. CO2-rich brine percolation experiments through Heletz reservoir rock samples (Israel): Role of the flow rate and brine composition. Int. J. Greenh. Gas Control in press.
Marcon, V., Kaszuba, J.P., 2015. Carbon dioxide–brine–rock interactions in a carbonate reservoir capped by shale: Experimental insights regarding the evolution of trace metals. Geochimica et Cosmochimica Acta 168, 22-42.
Martin, M., Wakefield, M., Bianchi, V., Esterle, J., Zhou, F., 2018. Evidence for marine influence in the Lower Jurassic Precipice Sandstone, Surat Basin, eastern Australia. Australian Journal of Earth Sciences 65, 75-91.
Matter, J.M., Stute, M., Snæbjörnsdottir, S.Ó., Oelkers, E.H., Gislason, S.R., Aradottir, E.S., Sigfusson, B., Gunnarsson, I., Sigurdardottir, H., Gunnlaugsson, E., Axelsson, G., Alfredsson,

H.A., Wolff-Boenisch, D., Mesfin, K., Taya, D.F.d.l.R., Hall, J., Dideriksen, K., Broecker, W.S., 2016. Rapid carbon mineralization for permanent disposal of anthropogenic carbon dioxide emissions. Science 352, 1312.
McCutcheon, J., Nothdurft, L.D., Webb, G.E., Shuster, J., Nothdurft, L., Paterson, D., Southam, G., 2017. Building biogenic beachrock: Visualizing microbially-mediated carbonate cement precipitation using XFM and a strontium tracer. Chem. Geol. 465, 21-34.
Palandri, J.L., Kharaka, Y.K., 2004. A compilation of rate parameters of water-mineral interaction kinetics for application to geochemical modeling. USGS Open File Report 2004-1068, p. 64.
Palandri, J.L., Rosenbauer, R.J., Kharaka, Y.K., 2005. Ferric iron in sediments as a novel CO2 mineral trap: CO2-SO2 reaction with hematite. Appl. Geochem. 20, 2038-2048.
Paterson, D., Jonge, M.D.d., Howard, D.L., Lewis, W., McKinlay, J., Starritt, A., Kusel, M., Ryan, C.G., Kirkham, R., Moorhead, G., Siddons, D.P., 2011. The X-ray Fluorescence Microscopy Beamline at the Australian Synchrotron. AIP Conference Proceedings 1365, 219-222.
Pauwels, H., Gaus, I., le Nindre, Y.M., Pearce, J., Czernichowski-Lauriol, I., 2007. Chemistry of fluids from a natural analogue for a geological CO2 storage site (Montmiral, France): Lessons for CO2-water-rock interaction assessment and monitoring. Appl. Geochem. 22, 2817-2833.
Pearce, J., Underschultz, J., La Croix, A., 2019a. Mineralogy, geochemical CO2-water-rock reactions and associated characterisation. The University of Queensland Surat Deep Aquifer Appraisal Project (UQ-SDAAP) Brisbane, Australia: The University of Queensland, 978-1-74272-251-1.
Pearce, J.K., Dawson, G.K.W., 2018 Gas-Water-Mineral Reactivity in Caprocks, in: S. Vialle, Ajo-Franklin, J., Carey, J.W. (Eds.), Geological Carbon Storage. doi: 10.1002/9781119118657.ch7.
Pearce, J.K., Dawson, G.K.W., Golab, A., Knuefing, L., Sommacal, S., Rudolph, V., Golding, S.D., 2019b. A combined geochemical and μCT study on the CO2 reactivity of Surat Basin reservoir and cap-rock cores: Porosity changes, mineral dissolution and fines migration. Int. J. Greenh. Gas Control 80, 10-24.
Pearce, J.K., Golab, A., Dawson, G.K.W., Knuefing, L., Goodwin, C., Golding, S.D., 2016. Mineralogical controls on porosity and water chemistry during O2-SO2-CO2 reaction of CO2 storage reservoir and cap-rock core. Appl. Geochem. 75, 152-168.
Pearce, J.K., Kirste, D.M., Dawson, G.K.W., Farquhar, S.M., Biddle, D., Golding, S., Rudolph, V., 2015. SO2 Impurity Impacts on Experimental and Simulated CO2-Water-Reservoir Rock Reactions at Carbon Storage Conditions. Chem. Geol. 399, 65-86.
Pearce, J.K., Kirste, D.M., Dawson, G.K.W., Rudolph, V., Golding, S.D., 2019c. Geochemical modelling of experimental O2–SO2–CO2 reactions of reservoir, cap-rock, and overlying cores. Appl. Geochem. 109, 104401.
Pearce, J.K., La Croix, A.D., Brink, F.J., Hayes, P.J., Underschultz, J.R., 2021. CO2 mineral trapping comparison in different regions: predicted geochemical reactivity of the Precipice Sandstone reservoir and overlying Evergreen Formation. Petroleum Geoscience 27, petgeo2020-2106.
Pearce, J.K., La Croix, A.D., Underschultz, J.R., Golding, S.D., 2020. Long term reactivity of CO2 in a low salinity reservoir-seal complex. Appl. Geochem. 114, 104529.
Pirrie, D., Butcher, A.R., Power, M.R., Gottlieb, P., Miller, G.L., 2004. Rapid quantitative mineral and phase analysis using automated scanning electron microscopy (QemSCAN); potential applications in forensic geoscience. Geological Society, London, Special Publications 232, 123-136.
Porter, R.T.J., Fairweather, M., Pourkashanian, M., Woolley, R.M., 2015. The range and level of impurities in CO2 streams from different carbon capture sources. Int. J. Greenh. Gas Control 36, 161-174.

Ryan, C.G., Siddons, D.P., Kirkham, R., Dunn, P.A., Kuczewski, A., Moorhead, G., De Geronimo, G., Paterson, D.J., De Jonge, M.D., Hough, R.M., Lintern, M.J., Howard, D.L., Kappen, P., Cleverley, J., 2010. The new Maia detector system: Methods for high definition trace element imaging of natural material, AIP Conference Proceedings, pp. 9-17.
Ryan, C.G., Siddons, D.P., Kirkham, R., Li, Z.Y., de Jonge, M.D., Paterson, D.J., Kuczewski, A., Howard, D.L., Dunn, P.A., Falkenberg, G., Boesenberg, U., De Geronimo, G., Fisher, L.A., Halfpenny, A., Lintern, M.J., Lombi, E., Dyl, K.A., Jensen, M., Moorhead, G.F., Cleverley, J.S., Hough, R.M., Godel, B., Barnes, S.J., James, S.A., Spiers, K.M., Alfeld, M., Wellenreuther, G., Vukmanovic, Z., Borg, S., 2014. Maia X-ray fluorescence imaging: Capturing detail in complex natural samples. Journal of Physics: Conference Series 499, 012002.
Steefel, C.I., 2001. GIMRT, version 1.2: Software for modeling multicomponent, multidimensional reactive transport. User's Guide, UCRL-MA-143182, Livermore, California: Lawrence Livermore National Laboratory.
Underschultz, J.R., Pasini, P., Grigorescu, M., de Souza, T.L., 2016. Assessing aquitard hydraulic performance from hydrocarbon migration indicators: Surat and Bowen basins, Australia. Marine and Petroleum Geology 78, 712-727.
Uysal, I.T., Golding, S.D., Bolhar, R., Zhao, J.-x., Feng, Y.-x., Baublys, K.A., Greig, A., 2011. CO2 degassing and trapping during hydrothermal cycles related to Gondwana rifting in eastern Australia. Geochimica et Cosmochimica Acta 75, 5444-5466.
Viswanathan, H., Dai, Z., Lopano, C., Keating, E., Hakala, J.A., Scheckel, K.G., Zheng, L., Guthrie, G.D., Pawar, R., 2012. Developing a robust geochemical and reactive transport model to evaluate possible sources of arsenic at the CO2 sequestration natural analog site in Chimayo, New Mexico. Int. J. Greenh. Gas Control 10, 199-214.
Wang, J., La Croix, A.D., Gonzalez, S., He, J., Underschultz, J., 2019. Sequence stratigraphic analysis of the Lower Jurassic Precipice Sandstone and Evergreen Formation in the Surat Basin, Australia: Implications for the architecture of reservoirs and seals for CO2 storage. Marine and Petroleum Geology 102, 829-843.
Watson, M., Gibson-Poole, C.M., 2005. Reservoir Selection for Optimised Geological Injection and Storage of Carbon Dioxide: A Combined Geochemical and Stratigraphic Perspective., FOURTH ANNUAL CONFERENCE ON CARBON CAPTURE AND SEQUESTRATION DOE/NETL, Virginia, US.
Watson, M.N., Zwingmann, N., Lemon, N.M., 2004. The Ladbroke Grove-Katnook carbon dioxide natural laboratory: A recent CO2 accumulation in a lithic sandstone reservoir. Energy 29, 1457-1466.
Wdowin, M., Tarkowski, R., Franus, W., 2014. Determination of changes in the reservoir and cap rocks of the Chabowo Anticline caused by CO2–brine–rock interactions. International Journal of Coal Geology 130, 79-88.
Wigley, M., Kampman, N., Dubacq, B., Bickle, M., 2012. Fluid-mineral reactions and trace metal mobilization in an exhumed natural CO2 reservoir, Green River, Utah. Geology 40, 555-558.
Wolhuter, A., Garnett, A., Underschultz, J., 2019. Notional injection site identification report, The University of Queensland Surat Deep Aquifer Appraisal Project –Supplementary Detailed Report, The University of Queensland.
Wunsch, A., Navarre-Sitchler, A.K., Moore, J., McCray, J.E., 2014. Metal release from limestones at high partial-pressures of CO2. Chem. Geol. 363, 40-55.
Xu, T.F., Apps, J.A., Pruess, K., 2005. Mineral sequestration of carbon dioxide in a sandstone-shale system. Chem. Geol. 217, 295-318.
Yuan, G., Cao, Y., Schulz, H.-M., Hao, F., Gluyas, J., Liu, K., Yang, T., Wang, Y., Xi, K., Li, F., 2019. A review of feldspar alteration and its geological significance in sedimentary basins: From shallow aquifers to deep hydrocarbon reservoirs. Earth-Science Reviews 191, 114-140.